https://doi.org/10.5194/nhess-2020-397
Preprint. Discussion started: 22 February 2021

Natural Hazards and Earth System Sciences
Discussions

Evaluation of Mei-yu Heavy-Rainfall Quantitative Precipitation Forecasts in Taiwan by A Cloud-Resolving Model for Three Seasons of 2012-2014

Chung-Chieh Wang[1], Pi-Yu Chuang[1*], Chih-Sheng Chang[1], Kazuhisa Tsuboki[2], Shin-Yi Huang[1], and Guo-Chen Leu[3]

[1] Department of Earth Sciences, National Taiwan Normal University, Taipei, Taiwan
[2] Institute for Space-Earth Environmental Research, Nagoya University, Nagoya, Japan
[3] Central Weather Bureau, Taipei, Taiwan

Corresponding author: Pi-Yu Chuang (giselle780507@hotmail.com), Department of Earth Sciences, National Taiwan Normal University. No. 88, Sec. 4, Ting-Chou Rd., Taipei, 11677 Taiwan.

https://doi.org/10.5194/nhess-2020-397
Preprint. Discussion started: 22 February 2021

Natural Hazards and Earth System Sciences
Discussions

Abstract

In this study, the performance of quantitative precipitation forecasts (QPFs) by the Cloud-Resolving Storm Simulator (CReSS) in real-time in Taiwan, at a horizontal grid spacing of 2.5 km and a domain size of 1500 × 1200 km^2, within a range of 72 h during three mei-yu seasons of 2012-2014 is evaluated using categorical statistics, with an emphasis on heavy events (≥ 100 mm per 24 h). The overall threat scores (TSs) of QPFs for all events on day 1 (0-24 h) are 0.18, 0.15, and 0.09 at the threshold of 100, 250, and 500 mm, respectively, and indicate considerable improvements compared to past results and 5-km models.

Moreover, the TSs are shown to be higher and the model more skillful in predicting larger events, in agreement with earlier findings for typhoons. After classification based on observed rainfall, the TSs of day-1 QPFs for the largest 4% of events by CReSS at 100, 250, and 500 mm (per 24 h) are 0.34, 0.24, and 0.16, respectively, and can reach 0.15 at 250 mm on day 2 (24-48 h) and 130 mm on day 3 (48-72 h). The larger events also exhibit higher probability of detection and lower false alarm ratio than weaker events almost without exception across all thresholds.

The strength of the model lies mainly in the topographic rainfall in Taiwan rather than migratory events that are less predictable. Our results highlight the crucial importance of cloud-resolving capability and the size of fine mesh for heavy-rainfall QPFs in Taiwan.

https://doi.org/10.5194/nhess-2020-397
Preprint. Discussion started: 22 February 2021

Natural Hazards and Earth System Sciences
Discussions

1 Introduction

The quantitative precipitation forecast (QPF) is one of the most challenging areas in modern numerical weather prediction (NWP; e.g., Golding, 2000; Fritsch and Carbone, 2004; Cuo et al., 2011), especially for extreme events that have high potential for hazards. With its steep and complex topography, Taiwan over the western North Pacific (Fig. 1) experiences extreme rainfall rather frequently mainly in two periods: the typhoon (July-October) and mei-yu (May-June) seasons (e.g., Kuo and Chen, 1990; Wu and Kuo, 1999; Jou et al., 2011; Chang et al., 2013), where landslides and flash floods in/near the mountains and flooding over low-lying plains and urban areas are the main hazards (e.g., Wang et al., 2012b, 2013b, 2016b). In order to better prepare for these hazards and reduce their impacts, model QPFs and their verifications, especially over heavy-rainfall thresholds from large events, are thus very important for Taiwan. Of course, to identify where the model can make significant improvements in QPFs and what approaches are effective to achieve them are also crucial (e.g., Clark et al., 2011).

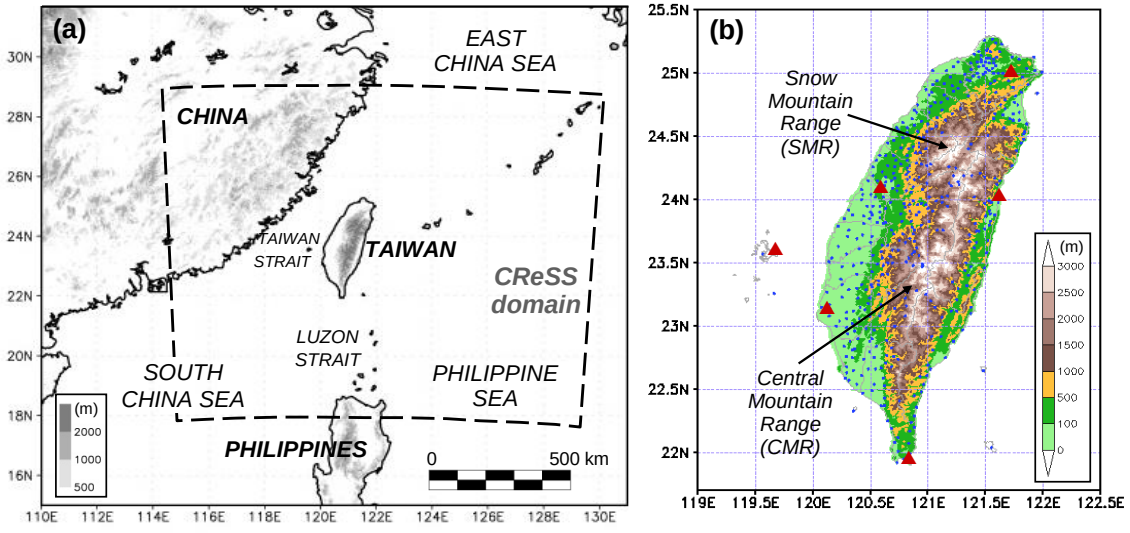

Figure 1. (a) The geography and topography (m, shading) surrounding Taiwan and the domain of 2.5-km CReSS (thick dashed box), and (b) the detailed terrain of Taiwan (m, color) and the locations of rain gauges (blue dots) and land-based radars (scarlet triangles) used to produce the reflectivity composites by the Central Weather Bureau (CWB). The two major mountain ranges in Taiwan, the Central Mountain Range (CMR) and Snow Mountain Range (SMR), are marked in (b).

https://doi.org/10.5194/nhess-2020-397
Preprint. Discussion started: 22 February 2021


Natural Hazards and Earth System Sciences Discussions

For the mei-yu season in Taiwan, earlier studies mainly employed the widely-used, standard categorical measures (see Section 2.4) to evaluate the performance of models such as the Mesoscale Model version 5 (MM5) at thresholds up to 50 mm per 12 h (e.g., Chien et al., 2002, 2006; Yang et al., 2004). Their results show that the models at the time had some skill in predicting rainfall occurrence at thresholds ≤ 2.5 mm, but little skill at 50 mm and above. In recent years, several studies (e.g., Hsu et al., 2014; Li and Hong, 2014; Su et al., 2016; Huang et al., 2016) have also examined the QPFs by the Weather Research and Forecasting (WRF) model (Skamarock et al., 2005) running at the Central Weather Bureau (CWB), including its ensembles at 5-km grid spacing (Δx). These studies indicate improvements over earlier models at thresholds up to 50-100 mm (per 12 h) over the previous decade. However, the skill at 150-200 mm and beyond is still limited, even with probability-matching (e.g., Ebert, 2001) within the forecast range of 24 h (see e.g., Figs. 9 and 10 of Huang et al., 2016). While the scores at the CWB will be compared with our results later, effective strategies and methods to improve the skill level of NWPs at thresholds near 100-150 mm and beyond are obviously much needed.

Wang (2015, hereafter referred to as W15) evaluated the QPFs, within 3 days, by a cloud-resolving model (CRM), the Cloud-Resolving Storm Simulator (CReSS; Tsuboki and Sakakibara, 2002, 2007), for all 15 typhoons to hit Taiwan in 2010-2012. With Δx = 2.5 km, a grid size comparable to research (e.g., Wang et al., 2005, 2011; 2013a, also Bryan et al., 2003; Done et al., 2004; Clark et al., 2007; Roberts and Lean, 2007), these deterministic forecasts show superior performance in QPFs, with threat scores (TSs, defined in Section 2.4) of 0.38, 0.32, and 0.16 at thresholds of 100, 250, and 500 mm, respectively, for all typhoons on day 1 (0-24 h, cf. his Fig. 13). Even on day 3 (48-72 h), the corresponding TSs are 0.21, 0.12, and 0.01. Thus, the skill by this CRM over the thresholds of 100-500 mm is remarkably high for typhoon rainfall in Taiwan.

Moreover, as summarized in Wang (2016, hereafter W16), W15 found a strong positive dependency of categorical scores on overall rainfall amount (or event magnitude). That is, the more rain, the higher the scores, and the better the model performs. For example, the TSs at the same thresholds (100, 250, and 500 mm) for his top-5 events (roughly top 5%) on day 1 are 0.68, 0.49, and 0.24, respectively (Fig. 1 of W16), all at least 1.5 times higher than their counterparts for all typhoons. An important implication of this finding is that the model QPFs for extreme events, *may not* be accurately assessed through categorical statistics without proper classification

https://doi.org/10.5194/nhess-2020-397
Preprint. Discussion started: 22 February 2021


Natural Hazards and Earth System Sciences Discussions

to isolate them from ordinary events, and particularly not by taking arithmetic mean of TSs of multiple forecasts. Wang (2015) also predicts the dependency, as a fundamental property, to exist in other rainfall regimes. For mei-yu rainfall in Taiwan, we are certainly keen to find out how this CRM performs, especially for the extreme events. Therefore, the main purpose of the current study is three-fold: 1) to assess the skill of the 2.5-km CReSS in predicting mei-yu rainfall, 2) to clarify whether the dependency property in categorical scores in the mei-yu regime in Taiwan and further evaluate the model QPFs for larger and extreme events, and 3) if the QPFs by CReSS prove to be superior to those reviewed above, why or where its strength lies? To answer these questions above are our objectives.

In Section 2, the model, data, and methodology are described. In Section 3, the overall scores of QPFs for groups with different event magnitudes are presented and compared with previous results. Then in Section 4, examples are selected to illustrate how the CRM performs in real-time forecasts and where its strength lies. Aspects related to the dependency property are further discussed in Section 5, and our conclusions are given in Section 6.

2 Data and Methodology

2.1 The CReSS model and its forecasts

The CReSS model is a non-hydrostatic, compressible CRM with a single domain and no nesting (Tsuboki and Sakakibara, 2002, 2007), and it has been used for weather forecasts in Taiwan since 2006 (http://cressfcst.es.ntnu.edu.tw/, W15; Wang et al., 2013, 2016a). Starting from July 2010, a grid size of 2.5 km is utilized, with a domain of 1500×1200 km^2 since May 2012 (Fig. 1a and Table 1). In CReSS, cloud formation, development, and all related processes are explicitly treated using a bulk cold-rain microphysical scheme with six species: vapor, cloud water, cloud ice, rain, snow, and graupel without any cumulus parameterization scheme. Other sub-grid scale processes parameterized in the model include turbulent mixing in the planetary boundary layer, as well as surface radiation and momentum/energy fluxes. These physical options are identical to W15, and also given in Table 1.

The operational analyses and forecasts by the Global Forecasting System (GFS, Kanamitsu, 1989; Kalnay et al., 1990; Moorthi et al., 2001; Kleist et al., 2009) of the National Centers for Environmental Prediction (NCEP), produced every 6 h (at 26 levels) were used as initial and

https://doi.org/10.5194/nhess-2020-397
Preprint. Discussion started: 22 February 2021


Natural Hazards and Earth System Sciences Discussions

boundary conditions (IC/BCs) for CReSS (Table 1), which are also run four times a day, each out to 72 h (now 78 h). At the lower boundary, terrain data at 30" resolution (roughly 900 m) and the NCEP analyzed sea surface temperature (SST) are also provided. With its limited domain size, the atmospheric evolution in CReSS is highly dictated by the NCEP forecasts, especially at longer ranges. Note that since 2013, the IC/BCs from the GFS have doubled the resolution from 1° × 1° to 0.5° × 0.5°, but all other settings are kept the same during our study period (Table 1).

Table 1. The basic configuration, initial/boundary conditions (IC/BCs), and physical packages of the 2.5-km CReSS used for real-time operation in 2012-2014.

Season	2012	2013 and 2014
Projection	Lambert Conformal (center at 120°E, secant at 10°N and 40°N)	
Grid spacing (km)	2.5 × 2.5 × 0.2-0.663 (0.5)*	
Grid dimension (x, y, z)	600 × 480 × 40	
Domain size (km)	1500 × 1200 × 20	
Forecast frequency	Every 6 h (at 0000, 0600, 1200, and 1800 UTC)	
Forecast range	72 h	78 h
IC/BCs (including SST)	NCEP GFS analyses/forecasts (at 26 levels)	
	1° × 1°	0.5° × 0.5°
Topography	Real at (1/120)° spatial resolution	
Cloud microphysics	Bulk cold-rain scheme (Lin et al., 1983; Cotton et al., 1986; Murakami, 1990; Ikawa and Saito, 1991; Murakami et al., 1994)	
PBL/turbulence	1.5-order closure with prediction of turbulent kinetic energy (Deardorff, 1980; Tsuboki and Sakakibara, 2007)	
Surface processes	Energy/momentum fluxes, shortwave and longwave radiation (Kondo, 1976; Louis et al., 1982; Segami et al., 1989)	
Substrate model	41 levels, every 5 cm to 2 m	

* The vertical grid spacing of CReSS is stretched (smallest at bottom), and the averaged spacing is given in the parentheses.

2.2 Data

The observational data used include synoptic weather maps from the CWB, the vertical maximum indicator (VMI) reflectivity composites every 30 min from land-based radars, and hourly rainfall data from about 440 gauges in Taiwan (Fig. 1b) for QPF verification. Along with NCEP gridded final analyses (on 1° × 1° grid), the weather maps are used to identify and

https://doi.org/10.5194/nhess-2020-397
Preprint. Discussion started: 22 February 2021


Natural Hazards and Earth System Sciences Discussions

synthesize the occurrence of favorable factors to heavy rainfall among events with different magnitude (to be described in Section 2.3). For selected heavy-rainfall cases, the radar composites are compared with the CReSS forecasts to assess the quality of the QPFs in Section 4.

2.3 Verification period classification

In this study, objective categorical statistics (e.g., Schaefer, 1990; Wilks, 2011) are used to verify QPFs mainly because: 1) the ability of models to predict the heavy rainfall at the correct location is imperative in Taiwan, since its primary hazards are landslides and floods, and 2) our results can be easily compared with earlier studies. Here, 24-h QPFs are chosen because: 1) the bulk rainfall accumulation from mei-yu events, as for typhoons, is our main concern rather than the rain over shorter periods, especially at longer ranges (days 2-3), and 2) the issue of double penalty on high-resolution QPFs (e.g., Ebert and McBride, 2000) is less serious using a longer accumulation period. Although the CReSS forecasts are made four times a day, only those from 0000 and 1200 UTC are evaluated in this study.

Table 2. The classification criteria using (at least) 10% of rain gauges with highest 24-h accumulated rainfall (0000-2400 or 1200-1200 UTC) over Taiwan, and the results in the number of 24-h segments (and percentage) and total points (sites) of $H + M + FA$ at selected rainfall thresholds (mm) for the different groups. During the mei-yu seasons of 2012-2014, the total N is 148776 and on average there are 442 rain gauges per segment. The points of $H + M + FA$ are based on the statistics of day-1 (0-24 h) QPFs, and N is also given (with no threshold).

Group	Criterion (of 10% gauges)	No. of segments (%)	No. of all points (N)	No. of points ($H + M + FA$) at threshold (mm)			
				50	100	250	500
A+	≥ 130 mm (a subset of A)	13 (3.9)	5622	3807	2453	490	32
A	≥ 50 mm	61 (18.1)	26826	11000	4889	675	47
B	≥ 25 mm, but not A	75 (22.3)	33018	4279	1078	98	4
C	≥ 10 mm, but not B	88 (26.1)	38583	1675	281	10	3
D	≥ 1 mm, but not C	67 (19.9)	29267	266	32	0	0
X	< 1 mm	46 (13.6)	20067	59	20	4	0
All	A through D plus X	337 (100.0)	147761	17279	6300	787	54

https://doi.org/10.5194/nhess-2020-397
Preprint. Discussion started: 22 February 2021

Natural Hazards and Earth System Sciences Discussions

A total of 366 target segments (0000-2400 and 1200-1200 UTC) in May-June, 2012-2014 are classified into several groups based on the observed rainfall using the following criteria, as summarized in Table 2. Groups A, B, C, and D are those periods with at least 10% rain gauges reaching 50, 25-50, 10-25, and 1-10 mm, respectively, while group X is the remaining periods with little or no rain. The full classification results (Table 3) give a total of 337 segments, excluding those under typhoon influence. Groups A-D individually account for about 18-26% and are comparable in sample size, while the driest group X is about 14% (Tables 2 and 3). These five groups are exclusive to each other, and the results without classification will be referred to as the "all" group. From group A, a subset of A+ that has ≥ 10% sites reaching 130 mm is identified and represents the most-rainy 4% in our sample with the highest hazard potential. The spatial distribution of mean mei-yu rainfall per season in 2012-2014, with a peak amount of about 1700 mm, is shown in Fig. 2 and resembles the climatology (e.g., Yeh and Chen, 1998; Chien and Jou, 2004; Chi, 2006; Wang et al., 2017).

Table 3. The full classification result for all the 24-h verification periods during the three mei-yu seasons of 2012-2014. For each month, the first (second) row gives the results of 0000-2400 (1200-1200) UTC. While the groups of A-D and X are denoted by their corresponding letter, a bold A indicates group A+ (a subset of A) and T marks the periods influenced by tropical cyclones and thus excluded from study.

Year	Month	Time (UTC)	Date in month			Segments included (A-D, X)
			1-10	11-20	21-31 (or 21-30)	
2012	May	0000	XAABDXXXBB	CCXXCBAAAB	XXDXDCAAABC	31
		1200	CAADXXXBCC	CXXCBBAB**A**D	XXXXDBAABBD	31
	Jun	0000	CCBCCCCB**AA**	**AA**AAABBTTT	TCCDDCTTTD	23
		1200	DBCDCDBA**AA**	**A**AAABBTTTT	TCDDDTTTTD	21
2013	May	0000	CCCCBBCCDA	AACCCABAA**A**	CBCCCDDDDDX	31
		1200	CCDCACCDD**A**	BBCCCABABA	BBCCDDDDDXX	31
	Jun	0000	XXCBCCXXCB	BBABCDDDXX	BDBCCXXXXD	30
		1200	XDBCCDXDCB	BABBDDDXXB	CBBCXXXXXD	30
2014	May	0000	CCBBBBCCCD	DCBD**A**BXBA**A**	ADDCDCCBBBC	31
		1200	CBDABCDCDD	CBDAAXBAA**A**	BDCCDBBABCD	31
	Jun	0000	XDACAABBBC	CTTTTTTDDB	DCBCCDXCAC	24
		1200	XACBAABBDC	TTTTTTTDBD	CCBCDXDBAC	23
Total			A+: 13, A: 61, B: 75, C: 88, D: 67, X: 46 (T: 29)			337

https://doi.org/10.5194/nhess-2020-397
Preprint. Discussion started: 22 February 2021

Natural Hazards and Earth System Sciences
Discussions

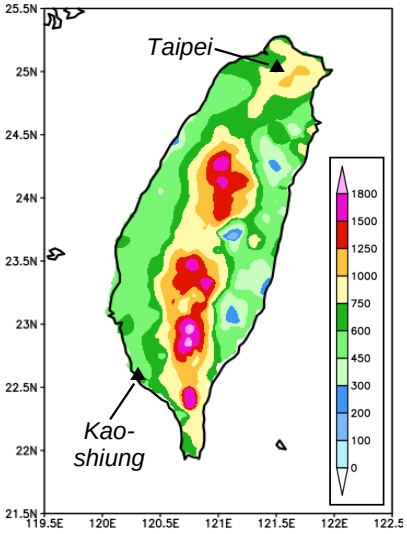

Figure 2. Spatial distribution of mean total rainfall (mm) per mei-yu season (1 May through 30 Jun) in 2012-2014. The cities of Taipei and Kaoshiung are marked.

2.4 Categorical measures of model QPFs

As mentioned, the 24-h QPFs by CReSS are verified against the rain gauge data, at three different ranges of 0-24, 24-48, and 48-72 h (days 1-3). For this purpose, objective skill scores computed from the standard 2 × 2 contingency table (or the categorical matrix) at 14 thresholds from 0.05 to 750 mm are adopted. These measures include the TS (also called critical success index), bias score (BS), probability of detection (POD), and false alarm ratio (FAR), respectively defined as (e.g., Schaefer, 1990; Wilks, 2011; Ebert et al., 2003; Barnes et al., 2009)

$$\mathrm{TS} = H/(H + M + FA), \quad (1)$$

$$\mathrm{BS} = (H + FA)/(H + M) = F/O, \quad (2)$$

$$\mathrm{POD} = H/(H + M) = H/O, \text{ and} \quad (3)$$

$$\mathrm{FAR} = FA/(H + FA) = FA/F, \quad (4)$$

where H, M, and FA are the counts of hits (both observed and predicted), misses (observed but not predicted), and false alarms (predicted but not observed), respectively, among a total number of N verification points. Here, $N = H + M + FA + CN$, where CN is the correct negatives (neither observed nor predicted), and the total counts in observation (O) and forecast (F) are simply $O = H + M$ and $F = H + FA$. The values of TS, POD, and FAR are all bounded by 0 and 1, and the

https://doi.org/10.5194/nhess-2020-397
Preprint. Discussion started: 22 February 2021


Natural Hazards and Earth System Sciences Discussions

higher (lower) the better for TS and POD (FAR). For BS, its value can vary from 0 to ∞ (or N – 1 in practice), but unity is the most ideal. By interpolating the model QPFs onto the gauge sites that serve as verification points (i.e., $N \approx 440$ per segment) using the bi-linear method, the counts of *H*, *M*, *FA*, and *CN* at any given threshold can be easily obtained for each segment. Although the density of rain gauges varies to some extent (roughly every 5-10 km in the plains and ≥10-20 km in the mountains, cf. Fig. 1b), their weights are assumed equal (e.g., Wang, 2014). For any group (e.g., A+) at a given threshold, the scores are obtained from a single 2 × 2 table that combines the entries from all segments, so that the sample sizes are maximized (cf. Table 2, e.g., W15, W16). This practice also remedies the issue of sampling in-homogeneity and increases the stability of results, especially toward the high thresholds, as long as the points involved in the matrix are not too few in number (cf. Table 2). Since neither the observation nor the forecast ever reached 750 mm (per 24 h) during the study period, results up to 500 mm (the next highest threshold) are presented in later sections. Also, only 24-h QPFs are evaluated in the current study. Except for the categorical matrix, subjective visual verification is also used in the selected examples (Section 4).

3 Mei-yu QPFs in 2012-2014

3.1 Overall skill by the 2.5-km CReSS

Following the method described above, the categorical matrices across the thresholds are obtained and the overall skill of CReSS in mei-yu QPFs during 2012-2014 is shown in Fig. 3 using the performance diagram. Proposed by Roebber (2009), the diagram uses the success ratio (SR = 1 – FAR = *H*/*F*) and POD as its two axes, and can also depict the TS (gray curved isopleths, higher toward upper-right) and BS (brown dotted lines) simultaneously. In Fig. 3, the scores from forecasts at both 0000 and 1200 UTC for segments (of 24 h) in groups A+, A to D, and all periods (A-D plus X, cf. Table 2) are shown for ranges of day 1, 2, and 3, respectively. The "all" group (black) shows the overall skill for all mei-yu rainfall without classification, and its TS for day-1 QPFs decreases slowly from 0.6 at 0.05 mm to 0.18 at 100 mm, 0.15 at 250 mm, and 0.09 at 500 mm (Fig. 3a). Over heavy-rainfall thresholds ≥ 160 mm, the TSs of 0.09-0.16 are significantly higher than those reviewed in section 1. Even on day 2, the TSs remain at 0.11 to 0.06 over 160-500 mm, and above 0.03 up to 350 mm on day 3 (Figs. 3c,e).

https://doi.org/10.5194/nhess-2020-397
Preprint. Discussion started: 22 February 2021


Natural Hazards and Earth System Sciences
Discussions

When all segments are stratified by the observed event magnitude, the TSs are higher and the skill better for larger events than smaller ones, following the order of A+ then A to D for all thresholds at all three ranges without any exception (Fig. 3), while each individual curve mostly decreases with threshold when rain areas reduce in size (as shown in Fig. 4). Thus, the positive dependency of categorical measures on rainfall amount is also strong and evident in mei-yu QPFs in Taiwan, as predicted by W15. Linked to this dependency, the TSs for large events are also higher than those for the "all" group from the entire sample. For the most hazardous group A+, for example, the TS on day 1 is 0.34 at 100 mm, 0.24 at 250 mm, and 0.16 at 500 mm (per 24 h, Fig. 3a). On days 2 and 3, the corresponding TSs are 0.32, 0.15, and 0.07 (Fig. 3c), and 0.25, 0.05, and 0.00 (Fig. 3e), respectively, all higher than their counterparts for the all group (except day 3 at 500 mm). If we select TS ≥ 0.15 to indicate some predictive skill, then the QPFs by the 2.5-km CReSS have skill all the way up to 500 mm (per 24 h) on day 1, 250 mm on day 2, and 130 mm on day 3. Also, for A+, A, and all groups, the TSs of day-2 QPFs stay quite close to the values on day 1, and some are even identical, from low thresholds up to 200-250 mm. For day-3 QPFs compared to day 2, the same is true up to about 130 mm (Fig. 3, left column). Such results that some skill of heavy-rainfall QPFs still exists on days 2-3 are very encouraging. On the other hand, at thresholds ≥ 50 mm, the skill for B-D events (Fig. 3, right column) are limited (TS ≤ 0.08) when the rain areas are relatively small (with $O/N \leq 6\%$, Fig. 4), but as discussed in W15, this is not important due to low hazard potential.

Another fairly subtle but important feature in Fig. 3 is that the TSs of all, A, and A+ groups decrease only marginally at times, or do not drop at all, across some heavy-rainfall thresholds, particularly on days 1-2, despite the reduction in rain-area size (left column). Some examples include the TSs for group A+ over 100-350 mm on day 1 (drops from 0.34 to 0.21), and those for group A over the same thresholds on day 1 (from 0.23 to 0.15) and over 100-250 mm on day 2 (from 0.20 to 0.14). Even on day 3, the decrease of A and "all" curves from 160 to 350 mm is rather slow, although the TSs there are only 0.03-0.07 (Fig. 3e). Such a slow decline in TSs with thresholds indicates that in a relative sense, the model is more capable to produce hits toward the rainfall maxima, which occur more frequently in the mountains (cf. Figs. 1b and 2).

https://doi.org/10.5194/nhess-2020-397
Preprint. Discussion started: 22 February 2021

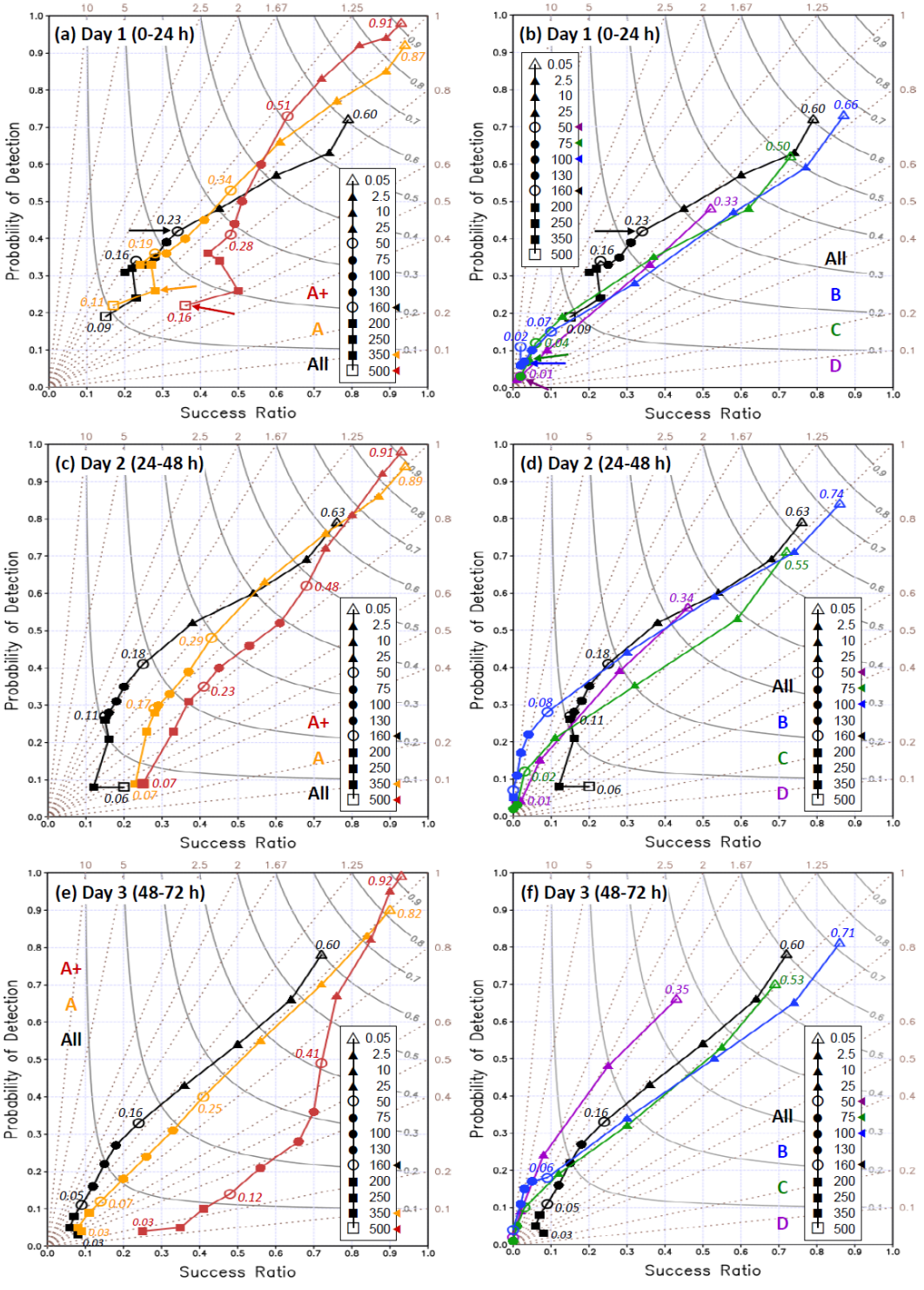

https://doi.org/10.5194/nhess-2020-397
Preprint. Discussion started: 22 February 2021


Natural Hazards and Earth System Sciences Discussions

248 **Figure 3.** Performance diagrams of 24-h QPFs for (a),(b) day 1 (0-24 h), (c),(d) day 2 (24-48 h), and (e),(f) day 3
249 (48-72 h) by the 2.5-km CReSS, at 13 rainfall thresholds (inserts) from 0.05 to 500 mm, during three mei-yu seasons
250 (May-Jun) in 2012-2014 in Taiwan. Results for groups A+, A, and All (All, B, C, and D) are plotted in left (right)
251 column with different colors. TS values (rounded to two decimal places) are labelled at fixed thresholds of 0.05, 50,
252 160, and 500 mm (open symbols) or selected endpoints (smaller fonts), and data points with TS = 0 at high
253 thresholds are omitted. For each group, the threshold where the observed rain-area size (*O*/*N*) falls below 1% is
254 labeled in insert, and also marked by an arrow in (a),(b).
255
256 By definition, both POD and SR cannot be lower than the TS [cf. Eqs. (1), (3), and (4)], and
257 the ratio of POD/SR equals to the BS (thus, POD < SR if BS < 1 and vice versa). In Fig. 3, the
258 PODs start at 0.05 mm from nearly perfect values of 0.98-0.99 for days 1-3 for group A+, at least
259 0.9 for A, and ≥ 0.72 for all segments (left column). For these three groups, the PODs at 250 mm
260 remain at least 0.32 on day 1, 0.21 on day 2, and 0.05 on day 3. Like the TS, the skill in POD for
261 mei-yu rainfall indeed decreases quite significantly with forecast range (lead time), particularly
262 toward high thresholds, mainly due to error growth and the reduction in predictability, but some
263 skill still exists at 130 mm even on day 3, with POD = 0.16 and TS = 0.07 (for all segments). The
264 SR values (and thus FAR) are again the best for group A+ and ≥ 0.36 across all thresholds on
265 day 1, including 500 mm (Fig. 3a). On day 2, the SRs for A+ over 130-500 mm decrease but not
266 by too much, and the values over 10-250 mm even increase on day 3 (Figs. 3c,e). Often, the SR
267 for A+ is considerably higher than those for A and all events regardless of forecast range,
268 particularly over heavy-rainfall thresholds. Overall, the model also produces higher POD and SR
269 (i.e., lower FAR) for larger events compared to smaller ones at all thresholds and all three
270 forecast ranges in Fig. 3, with only a few exceptions after close inspection. Therefore, as for
271 typhoon rainfall (W15), the 2.5-km CReSS is the most skillful in predicting the largest events in
272 the mei-yu season in Taiwan..
273 Next, the BS values are examined for over/under-prediction (i.e., above/below the diagonal
274 line) in Fig. 3, where the threshold with *O*/*N* falling below 1% is marked to indicate values that
275 might be potentially unstable and less meaningful. For day-1 QPFs, the BSs for all segments
276 suggest slight under-prediction over low thresholds ≤ 10 mm (per 24 h), but some over-
277 prediction (BS ≈ 1.25-1.5) across 50-350 mm (Fig. 3a). On the contrary, the model shows slight
278 over-prediction over 0.05-75 mm for the largest events of group A+ (with BSs up to 1.15), but
279 under-prediction toward higher thresholds, with the lowest BS of 0.52 at 350 mm. Mostly

https://doi.org/10.5194/nhess-2020-397
Preprint. Discussion started: 22 February 2021

Natural Hazards and Earth System Sciences
Discussions

between the two curves mentioned above, the curve for group A stays closer to unity and is more ideal across nearly all thresholds (Fig. 3a). For B-D groups (Fig. 3b), their characteristics are similar to the All group, with BSs of 0.8-1.0 at low thresholds but generally some over-prediction across higher thresholds. However, their BS values rarely exceed 2.5, unless the *O*/*N* values drop to below 1%. The situation for BSs between different groups remains similar on days 2 and 3 (Figs. 3c-f), and the over-forecasting across the middle thresholds in group A (at all ranges) can be confirmed to come mainly from groups B-D, as groups A+ and A exhibit little or a much less tendency for over-prediction there (Fig. 3).

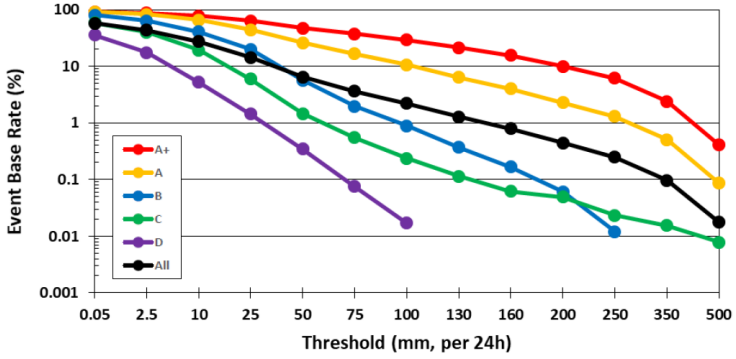

Figure 4. Observed rain-area size or base rate (*O*/*N*, %) of 24-h rainfall (same for days 1-3) in logarithmic scale used to compute the scores in Fig. 3

Toward the longer ranges of days 2 and 3, the BS values in general become smaller, particularly for the larger groups (Fig. 3, left column). Thus, the over-prediction in group A is reduced and the under-prediction in A+, which is the most important group, becomes more serious, especially toward the high thresholds (Figs. 3c,e). For example, the BS of day-2 QPFs for A+ is ideal and ≥ 0.8 up to 200 mm but declines to about 0.35 at 500 mm, but it is already below 0.4 at 130 mm on day 3. After closer inspection, the reason behind this behavior can be revealed as the following. Since group A+ is the observed top events that turned out to be very rainy, the atmosphere evolved in such a way to typically bring a greater number of favorable factors together in synergy to result in their occurrence. In model forecasts, when errors grow and the evolution deviates, the chance to become less rainy (not as favorable) is higher than more rainy, more so in forecasts made earlier at longer ranges. Thus, the probability to under-forecast peak rainfall rises with lead time. For smaller events that turned out to produce not much rainfall

https://doi.org/10.5194/nhess-2020-397
Preprint. Discussion started: 22 February 2021


Natural Hazards and Earth System Sciences Discussions

(i.e., B-D and X), a similar tendency does not exist or is weaker, and BS tends to be greater than unity. Thus, as exemplified here, the BSs from the larger and hazardous events can be quite different from those from all events, which are inevitably affected by the more frequent but small (unimportant) events. So, to say the least, one needs to practice caution in the interpretation of BS, which can also become unstable when O/N approaches zero (which inevitably happens at certain thresholds).

3.2 Improvement in heavy-rainfall QPFs

To assess the improvement in heavy-rainfall QPFs in mei-yu season made by the 2.5-km CReSS, our results are compared to those at the CWB for the same period. Figure 5 shows the TSs of day-1 (0-24 h) and day-2 (24-48 h) QPFs for May and June of 2013 and 2014 by the CWB WRF model and several products from their 20-member WRF ensemble prediction system (WEPS, e.g., Hong et al., 2015), all with Δx = 5 km, as an example. These plots are produced for each month at the CWB for routine verification (within a range of 48 h) since 2013, and are the same as those used by Huang et al. (2015, 2016). In addition to deterministic forecasts, the scores also include those using probability-matching techniques (PM and NPM, e.g., Ebert, 2001; Fang and Kuo, 2013), which may provide some benefit over the ensemble mean (WEPS) over thresholds of about 50-200 mm (e.g., Su et al., 2016; Huang et al., 2016). In Fig. 5, one can see that the TSs are no higher than 0.07 at 100 mm (per 24 h) and 0.03 at 200 mm (and TS = 0 ≥ 300 mm) for either day 1 or day 2 in the two mei-yu seasons of 2013 and 2014, in line with the review given in Section 1. Overall, the "all" curves in Fig. 3 indicate that the 2.5-km CReSS exhibits better skill than those reviewed in Section 1 (with Δx as fine as 5 km at most), especially at thresholds above 100 mm (e.g., TS = 0.15 at 250 mm and 0.09 at 500 mm for day 1). With even higher TSs for larger and more hazardous events (groups A and A+), the improvement of heavy-rainfall QPFs in the present study from earlier results is therefore significant and quite dramatic.

https://doi.org/10.5194/nhess-2020-397
Preprint. Discussion started: 22 February 2021

Natural Hazards and Earth System Sciences
Discussions

330

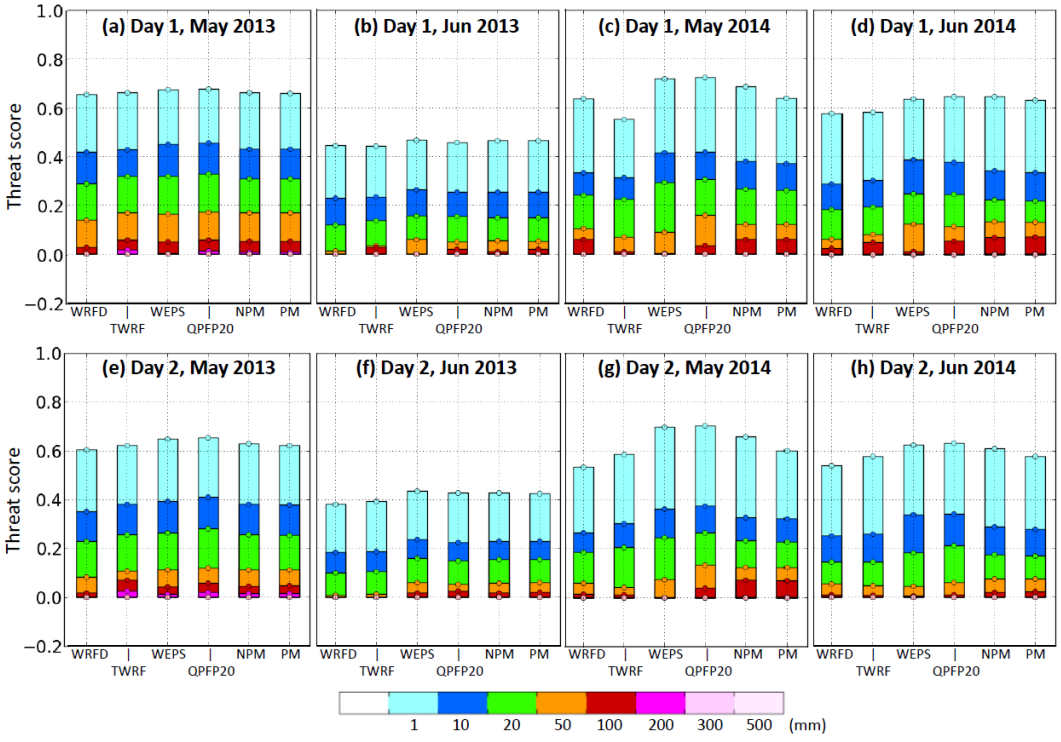

331 **Figure 5.** The TS of 0-24-h QPFs (day 1) for (a) May and (b) Jun of 2013, and (c) May and (d) Jun of 2014,
332 respectively, at selected thresholds over 1-500 mm (per 24 h, scale at bottom) by two deterministic forecasts from
333 WRF (WRFD) and the Typhoon WRF (TWRF) and four ensemble forecasts from the 20-member WRF Ensemble
334 Prediction System: ensemble mean (WEPS), top 20% (QPFP20), and WEPS employing the probability matching
335 (PM) and new PM (NPM) techniques. (e)-(h) As in (a)-(d), but showing the TS of 24-48-h QPFs (day 2),
336 respectively.

337

338 ## 4 Examples of Model QPFs

339 Given the success of the CRM in its overall performance shown above, some examples of
340 CReSS forecasts are selected and presented in this section for further examination and
341 discussion. The main goal here is two-fold: 1) To illustrate how the model behaves and captures
342 the rainfall with the corresponding scores in individual forecasts in detail, and thus 2) to identify
343 where such a CRM has high skill in QPF and where it has limitations in Taiwan, thereby to shed

https://doi.org/10.5194/nhess-2020-397
Preprint. Discussion started: 22 February 2021


Natural Hazards and Earth System Sciences Discussions

344 light on the source of skill seen in Fig. 3. Since our focus is on heavy rainfall, the event during 9-
345 12 June 2012, the largest during our study period, is chosen for illustration.
346 The event of 9-12 June 2012 spanned four days and contributes more than half the segments
347 in group A+ (7 in 13, cf. Table 3), and the model's performance in predicting this event is thus
348 highly relevant. In Fig. 6a, the observed 24-h rainfall distributions over Taiwan are shown every
349 12 h, from 1200-1200 UTC 8 June to 0000-2400 UTC 12 June 2012. Except for the first forecast
350 period, all seven segments are qualified as A+ and five have a 24-h peak rainfall over 500 mm
351 (those from 1200 UTC 9 June). Reminiscent to the season average (cf. Fig. 2), three rainfall
352 maxima from this lengthy event exist: over southern CMR, near the intersection of CMR and
353 SMR in central Taiwan, and over northern Taiwan (Fig. 6a). The rain at the two mountain
354 centers (cf. Fig. 1b) is much more persistent than that in northern Taiwan, which concentrated
355 mainly over a 10-h period beginning 1400 UTC 11 June (Wang et al., 2016b). The southwesterly
356 plains also received considerable rainfall, especially around 9 June (Fig. 6a).
357 The 24-h QPFs produced by the 2.5-km CReSS (at 0000 or 1200 UTC) in real time
358 targeting the same periods as in Fig. 6a, at the ranges of days 1-3 are presented in Figs. 6b-d,
359 with the general quality expressed by the TS at 100 mm (lower right corner inside panels) and
360 thickened outline for TS ≥ 0.15 at the threshold of 50, 100, 200, 350, or 500 mm. The day-1
361 QPFs (Fig. 6b) are made from the forecasts starting (with initial time t_0) at the time of the
362 heading, while day-2 (Fig. 6c) and day-3 QPFs (Fig. 6d) in the same column (i.e., for the same
363 target period) are those made 24 and 48 h earlier, respectively. In Fig. 6, this extreme and
364 lengthy event was generally well captured by the model, especially on day 1 where the overall
365 rainfall pattern and TS both tend to be better, as expected. The best day-1 QPF is for 0000-2400
366 UTC 10 June (TS = 0.68 at 100 mm and 0.40 at 500 mm), followed by the one for 1200 UTC 11-
367 12 June (TS = 0.59 at 100 mm and 0.29 at 500 mm, columns 4 and 7, Fig. 6b). At longer ranges
368 on days 2 and 3, the rainfall magnitudes produced over the mountains and southwestern plains
369 are also comparable to observations, but the event starts somewhat too early and becomes less
370 rainy during 10-11 June with apparent under-forecast (Figs. 6c,d). As a result, the TSs for the
371 segments starting at 1200 UTC 8 June and during 10-11 June (columns 1 and 4-7) mostly
372 increase from longer to shorter ranges, i.e., with better QPFs at later times. This relationship with
373 range, however, does not hold true for the other segments, among which the day-3 and day-2

https://doi.org/10.5194/nhess-2020-397
Preprint. Discussion started: 22 February 2021

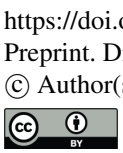

Natural Hazards and Earth System Sciences
Discussions
Open Access
EGU

374

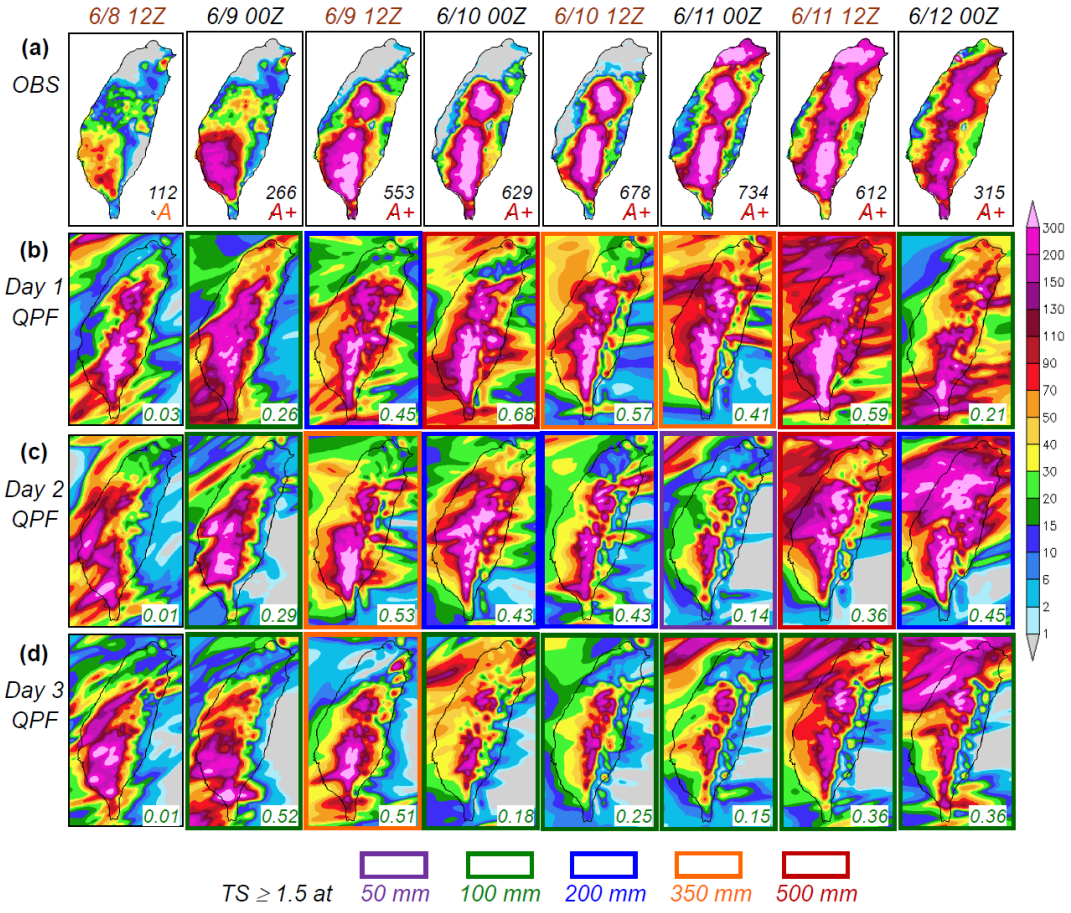

375 **Figure 6.** (a) The observed 24-h accumulated rainfall (mm, scale on the right) over Taiwan from 1200 UTC 8 Jun to
376 0000 UTC 13 Jun 2012, given every 12 h (from left to right), with the beginning time of accumulation (UTC)
377 labeled on top (black for 0000-2400 UTC and brown for 1200-1200 UTC). (b) Day-1 (0-24 h), (c) day-2 (24-48 h),
378 and (d) day-3 (48-72 h) QPFs valid for the same 24-h periods as shown in (a) by the 2.5-km CReSS (starting at
379 0000/1200 UTC under black/brown headings). In (a), peak 24-h rainfall (mm) and classification group are labeled.
380 In (b)-(d), thick boxes in purple, green, blue, orange, and scarlet denote forecasts having a TS ≥ 0.15 at the threshold
381 of 50, 100, 200, 350, and 500 mm (per 24 h), respectively, and the TS at 100 mm is also given (lower right corner).
382

383 QPFs for the period of 1200 UTC 9-10 June (TS ≥ 0.51-0.53 at 100 mm and 0.20-0.31 at 350
384 mm) and the day-2 QPF for 1200 UTC 11-12 June (TS = 0.40 at 500 mm) are particularly
385 impressive (columns 3 and 7). Compare to the rain over the terrain, the maximum across Taipei
386 in northern Taiwan during 11-12 June was largely over lower and flatter regions (cf. Figs. 1b and

https://doi.org/10.5194/nhess-2020-397
Preprint. Discussion started: 22 February 2021


Natural Hazards and Earth System Sciences
Discussions

2) and more challenging for the model to predict at the right location (Fig. 6), an aspect that will be further elaborated on later.

Figure 7 shows the TS and BS of day-1 to day-3 QPFs from the runs made at a series of initial times, including 1200 UTC of 7-9 June and the next four from 0000 UTC 10 to 1200 UTC 11 June (top to bottom), and our focus is mainly over the thresholds ≥ 100 mm. Inside the panels, the observed event base rate (O/N, i.e., rain-area size, identical for the same target period) and the hit probability (H/N, note that $H/N \leq O/N$) are given at selected points. With such information, it is easy to work out forecast base rate (F/N), POD, and SR, and thus how the model actually performed, particularly over the high thresholds. Some of the TSs at high thresholds mentioned above in relation to Fig. 6 can also be verified here.

Figures 7a-7f provide some examples on how the model did in predicting the commencement of the event (cf. Fig. 6, columns 1-3). As mentioned, the day-3 QPF made from 1200 UTC 7 June (Figs. 7a,b, blue curves) and day-2 QPF made one day later (Figs. 7c,d, red curves), both targeting 1200 UTC 9-10 June, are of fairly high quality. With rain areas (O/N) occupying 31%, 14%, and just 2% of Taiwan at 100, 200, and 350 mm, the day-2 QPF in Fig. 7c, with BS ≈ 0.6-1.1 (Fig. 7d), yields TSs of 0.53-0.31 at these thresholds. The day-3 QPF with t_0 at 1200 UTC 7 June, with less predicted rain and BS ≈ 0.3-0.6 (cf. Fig. 6d, column 3), the TSs are 0.51-0.2 (Figs. 7a,b). With TS at least 0.2 at 350 mm (an amount predicted only in southern CMR), both QPFs (for 1200 UTC 9-10 June) are quite skillful. Valid for periods with varying magnitude (B, A, and A+), the forecasts in Figs. 7a,b are also good examples to illustrate the dependency property (Fig. 3 and W15). In Figs. 7e,f, the TS curves at the three ranges (all for A+ events) are closer. In Fig. 8, the actual forecast near Taiwan between 42 and 69 h, from the run made at 1200 UTC 7 June, is compared with radar observations every 6 h to examine general rainfall locations. While a wind-shift line existed off eastern Taiwan, the surface mei-yu front was well to the north with prefrontal low-level southwesterly flow impinging on the island during this period (also Wang et al. 2016b). Active convection constantly developed over the mountains in central and southern Taiwan and moved from the upstream ocean into the southwestern plains, and this scenario was well captured by the 2.5-km CReSS (Fig. 8), yielding a high-quality QPF on day 3 despite some under-forecast at thresholds ≥ 75 mm (cf. Figs. 7a,b).

https://doi.org/10.5194/nhess-2020-397
Preprint. Discussion started: 22 February 2021

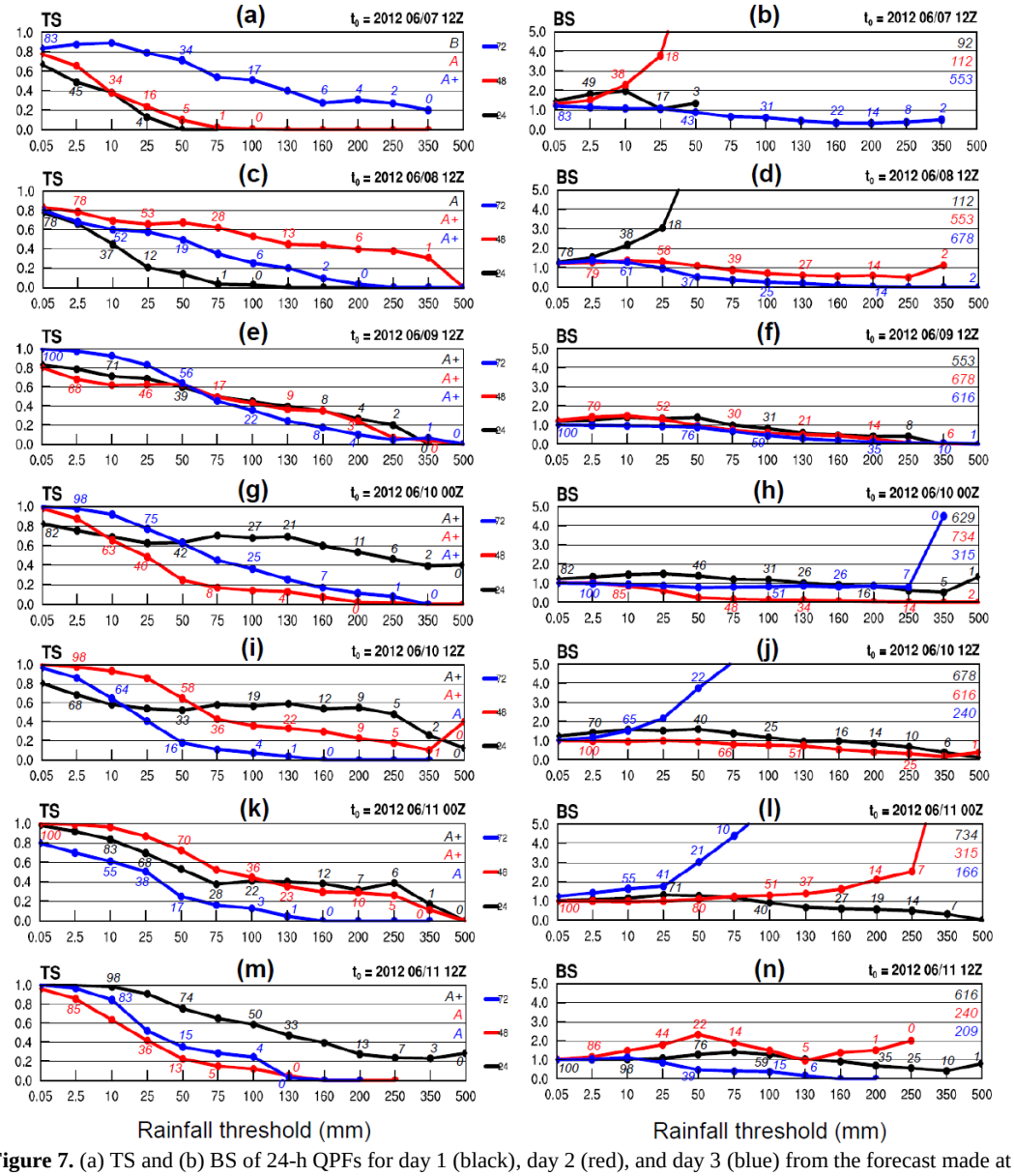

Figure 7. (a) TS and (b) BS of 24-h QPFs for day 1 (black), day 2 (red), and day 3 (blue) from the forecast made at 1200 UTC 7 Jun 2012 as a function of threshold (mm). (c),(d) to (m),(n) As in (a),(b), except for the forecasts made at 1200 UTC of (c),(d) 8 and (e),(f) 9 Jun, at (g),(h) 0000 UTC and (i),(j) 1200 UTC of 10 Jun, and (k),(l) 0000 UTC and (m),(n) 1200 UTC of 11 Jun, 2012, respectively. In left panels (for TS), the hit rate (*H*/*N*, %, rounded to integer) at selected points and the classification group for each day are labeled. In right panels (for BS), the observed base rate (*O*/*N*, %) and peak 24-h rainfall (mm) are also given.

https://doi.org/10.5194/nhess-2020-397
Preprint. Discussion started: 22 February 2021

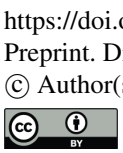

Natural Hazards and Earth System Sciences
Discussions

In the four following forecasts made on 10-11 June (Figs. 7g-n), while the dependency on event magnitude also exists, the QPFs made for A+ periods tend to have higher TSs above 75-100 mm at the shorter ranges (Figs. 7g,i,k), as mentioned. All of good forecast quality (cf. Figs. 6a,b, columns 4-7), the TSs of these day-1 QPFs can be as high as 0.48 at 250 mm and 0.40 at

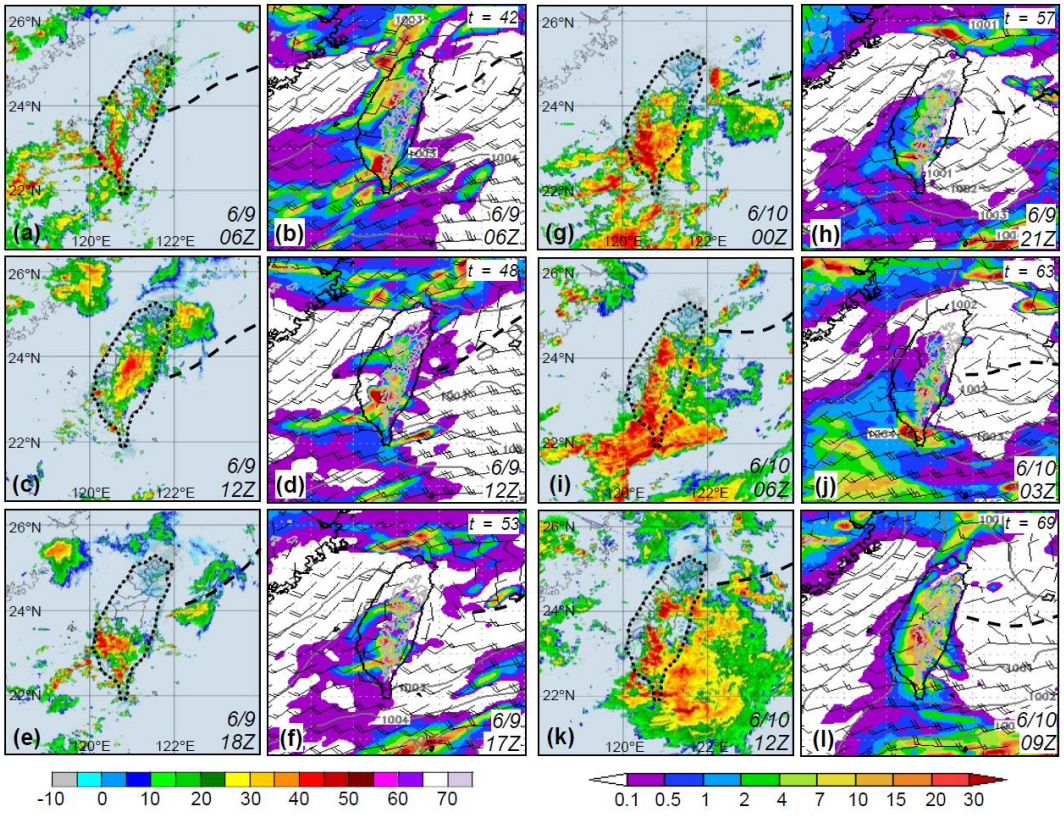

Figure 8. (First and third column) Radar reflectivity VMI composite (dBZ, scale at bottom left) in the Taiwan area (width roughly 600 km) every 6 h from (a) 0600 UTC 9 Jun to (k) 1200 UTC 10 Jun, 2012 (original plots provided by the CWB). (Second and fourth column) The CReSS forecast, starting from 1200 UTC 7 Jun 2012, of sea-level pressure (hPa, every 1 hPa, over ocean only), surface wind (kts, barbs, at 10 m), terrain height at 1 and 2 km (gray contours), and hourly rainfall (mm, color, scale at bottom right) valid at the time or within 3 h of the radar composite as labeled [in UTC (forecast time in h) at lower (upper) right corner] over the same area. The thick dashed lines mark the position of surface frontal or wind-shift line, based on NCEP gridded analyses for the observation (outline of Taiwan also highlighted).

https://doi.org/10.5194/nhess-2020-397
Preprint. Discussion started: 22 February 2021


Natural Hazards and Earth System Sciences Discussions

500 mm. At 350-500 mm, such high TS occurs with *O*/*N* below < 10% (or even only 1%), and thus indicates remarkable model accuracy in predicting the peak rainfall at the correct location in the mountains in this event. Over thresholds ≥ 200 mm, BS values in Fig. 7 indicate that under-prediction for this extreme event occurs much more often than over-prediction, while they also tend to be closer to unity (with less under-forecast) for QPFs achieving higher TSs. An over-prediction is more likely to happen for smaller events (A or below), across low thresholds below 50 mm, and/or when the rain area becomes small. In Fig. 7, for example, BS ≥ 2 at high thresholds for A+ group occurs only when *O*/*N* approaches zero (Figs. 7h,n), with the lone exception in Fig. 7l on day 2. Overall, the model does not have a tendency to over-predict such a large event (cf. Fig. 6).

The forecast on days 1-2 produced by the run starting at 1200 UTC 10 June is compared with radar observations in Fig. 9. Together with Fig. 8, the radar panels cover the wettest 72 h (0600 UTC 9-12 June) of the entire event. During day 1 (Figs. 9a-h), the scenario remains similar to Fig. 8, and the model again was able to capture the mountain rainfall. The convection moving in from the Taiwan Strait, however, was too active and the rain along the western coast on day 1 was over-predicted with BSs ≈ 1.2-1.6 from 0.05 up to 100 mm (cf. Fig. 7j). Note that in Fig. 7, some over-prediction across low thresholds can also exist for group A+ and lowers the TS, which otherwise can often exceed 0.8 at and below 25 mm. In any case, the model's performance over the low thresholds is of secondary importance.

Since 1200 UTC 11 June, the mei-yu front gradually approached northern Taiwan, and its western section moved rapidly across the island after about 0000 UTC 12 June (Figs. 9i-p). Studied by Wang et al. (2016b), the heavy rainfall in northern Taiwan (during 1400-2400 UTC) was caused by quasi-linear convection that developed south of the front (Figs. 9i,k,m), along a convergence zone between the low-level flow blocked and deflected by Taiwan's topography, and unblocked flow further to the northwest (but still prefrontal) in the environment (also e.g., Li and Chen, 1998; Yeh and Chen, 2002; Chen et al., 2005; Wang et al., 2005). In the model forecast, with apparent errors in the position and moving speed of the front (Figs. 9i-p), it is highly challenging to produce a similar system at the correct location and time even when the overall scenario surrounding northern Taiwan are reasonably predicted. In the simulation of

https://doi.org/10.5194/nhess-2020-397
Preprint. Discussion started: 22 February 2021

Natural Hazards and Earth System Sciences
Discussions

466

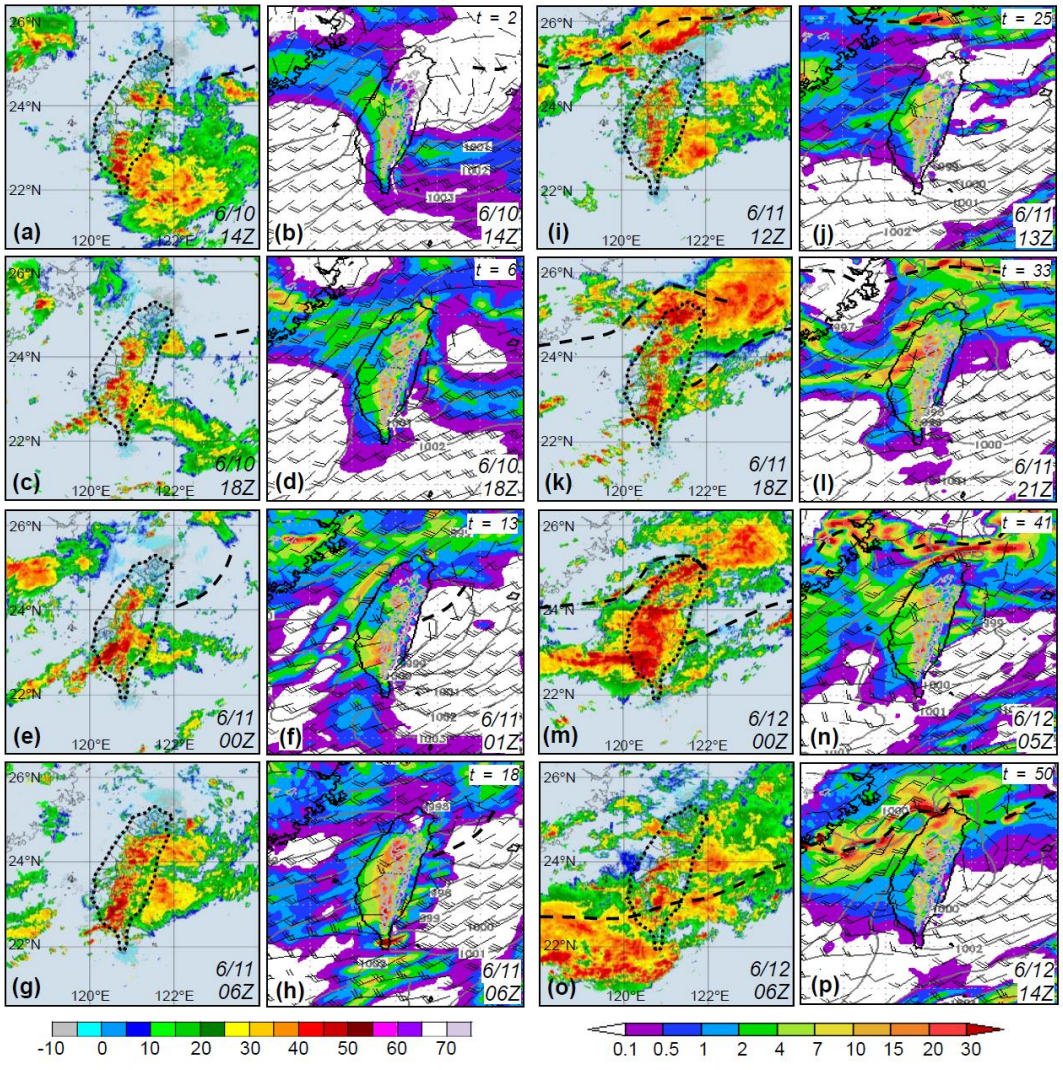

467 **Figure 9.** As in Fig. 8, but showing (columns 1 and 3) radar reflectivity composite (dBZ) at (a) 1400 UTC 10 Jun
468 and every 6 h from (c) 1800 UTC 10 Jun to (o) 0600 UTC 12 Jun, 2012, and (columns 2 and 4) the CReSS forecast,
469 starting from 1200 UTC 10 Jun 2012, of sea-level pressure (hPa), surface wind (kts), and hourly rainfall (mm) valid
470 at the time or within up to 8 h (towards the end) of the radar composite (as labeled).

471

472 Wang et al. (2016b), the rainbands cannot be fully captured even with a finer grid of Δx = 1.5 km
473 and the NCEP final analyses as IC/BCs. Thus, although the model did indicate a real possibility
474 of heavy rainfall in northern Taiwan in Fig. 9, the high TS of 0.4 at 500 mm on day 2 (Fig. 7i)
475 came from the mountains, where the rainfall is clearly more predictable (cf. Figs. 6a,c, column

https://doi.org/10.5194/nhess-2020-397
Preprint. Discussion started: 22 February 2021


Natural Hazards and Earth System Sciences Discussions

476 7), consistent with Walser and Schär (2004). Of course, the day-1 QPF with t_0 = 1200 UTC 11
477 June performed better in northern Taiwan than our example, but the goal here is to illustrate the
478 relatively high predictability of heavy rainfall phase-locked to the topography versus the low
479 predictability of rainfall produced by transient systems over low-lying plains.
480 The above example, together with other cases including those on 20 May 2013 and 20-21
481 May 2014, (cf. Table 3, not shown), suggests a lower predictability and a more challenging task
482 for QPFs produced by transient systems often in close association with the mei-yu front,
483 compared to topographic rainfall in Taiwan. Even though the overall scenario is reasonably and
484 realistically predicted (cf. Figs. 8 and 9), some position errors on the mei-yu front are almost
485 inevitable and the intrinsic predictability can limit the accuracy of the QPF. Also, for such
486 rainfall caused by transient systems, categorical statistics are known to be less effective in
487 verifying model QPFs (e.g., Davis et al., 2006; Wernli et al., 2008; Gilleland et al., 2010).
488 However, for the quasi-stationary, phase-locked rainfall over the topography in the majority of
489 large events (in both mei-yu and typhoon seasons, e.g., Chang et al., 1993; Cheung et al., 2008)
490 in Taiwan, they are still valid and useful as shown herein.
491

492 **5 Dependency of Skill Scores to Event Size**

493 In Section 3, a positive dependency in categorical measures by CReSS, including TS, POD,
494 and FAR, on rainfall amount is shown for the mei-yu regime in Taiwan, as predicted. Also
495 discussed in W15, this property arises mainly due to the positive correlation between the scores
496 and rain-area sizes, as given in Fig. 10 as an example with a correlation coefficient r = 0.89.
497 However, to explore whether the model is indeed more skillful in predicting larger rainfall
498 events, further analysis with the factor of rain-area size removed is needed. Different from W15,
499 our approach here is described below.
500 For each segment, the statistics (*H*, *M*, *FA*, and *CN*) at 13 fixed thresholds of 0.05-500 mm,
501 each occurring at a certain *O*/*N* (if the threshold ≤ the observed peak amount), are known. The
502 observed base rate (0-100%) is divided into bins every 5% except at 0-5%, where it is subdivided
503 into 0-0.5, 0.5-2, and 2-5% to give more comparable sample size. For each group (A+ or A-D),
504

https://doi.org/10.5194/nhess-2020-397
Preprint. Discussion started: 22 February 2021

Natural Hazards and Earth System Sciences
Discussions

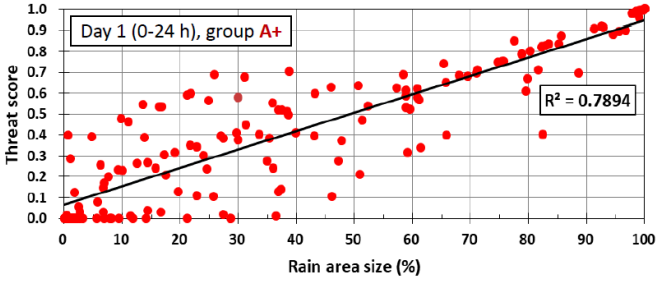

505 **Figure 10.** Scatter plot of TS versus observed rain-area size (%) from day-1 QPFs for group A+ from 0% to 100%
506 (from high to low rainfall threshold). The square of correlation coefficient (R^2) is given.
507

508 the statistics are then summed for each bin regardless of their rainfall threshold. Thus, those in
509 the same bin come from rain areas with similar sizes. In Fig. 11a, the distribution of total counts
510 of thresholds across O/N is plotted, and the larger events toward A+ are more capable to produce
511 rain areas larger in size (say, ≥60% of Taiwan). Also, the counts remain mostly around 50 for
512 $O/N \geq 40\%$, then rise to 200-300 with $O/N \leq 10\%$.

513 Due to fewer samples at larger O/N values, the TSs for different groups (from a single 2×2
514 table for each bin) are presented only for $O/N \leq 40\%$ in Figs. 10b-d. While the scores for B-D are
515 roughly the same, the TSs for A are clearly higher compared to them on day 1, and those for A+
516 are again higher compared to A on days 1 and 2 over most part of this range, sometimes by 0.05-
517 0.1, when the factor of rain-area size is removed (Figs. 10b,c). On day 3 (Fig. 10d), however, the
518 TSs for larger events (A+ and A) show no particular advantage. Therefore, similar to typhoons in
519 W15, the 2.5-km CReSS is more skillful in predicting the larger mei-yu events in Taiwan within
520 2 days, over the heavy-rainfall area (again, more likely over the mountains).

521 The higher TSs and better skill for large events at O/N within 40% (Fig. 10) are most likely
522 linked to the more favorable conditions at synoptic to meso-α scale, which the model is capable
523 to capture with higher accuracy (e.g., Walser and Schär, 2004). To briefly elaborate on this
524 aspect, seven items on the checklist used by CWB forecasters in the mei-yu season as a guidance
525 to issue heavy-rainfall warning (e.g., Wang et al., 2012a) are selected, and their occurrence
526 frequency, judged using surface weather maps and NCEP gridded analyses at the starting time of
527 each 24-h periods are summarized for different groups. These items include: 1) presence of
528 surface mei-yu front inside 20°-28°N, 118°-124°E; 2) Taipei (cf. Fig. 2) within 200 km south
529

https://doi.org/10.5194/nhess-2020-397
Preprint. Discussion started: 22 February 2021

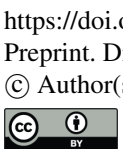

Natural Hazards and Earth System Sciences
Discussions

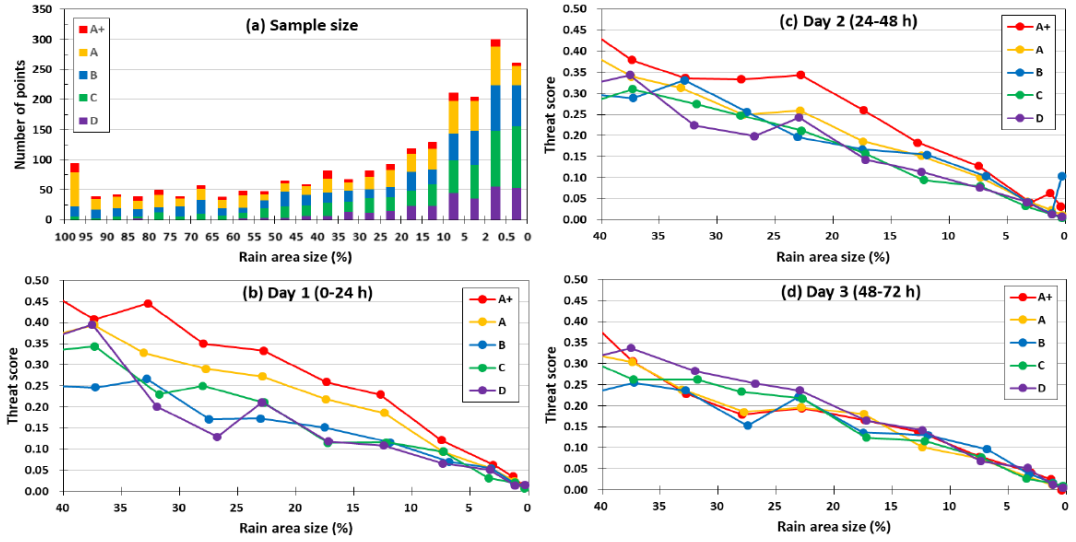

Figure 11. (a) The distribution of data points in the bins of observed rain-area size (%, every 5% from 100% to 5%, then 2-5%, 0.5-2%, and < 0.5%; same for days 1-3) among groups A+ and A to D. (b)-(d) The TS of 24-h QPFs for (b) day 1 to (d) day 3, respectively, as a function of observed rain-area size between 40% and 0%.

and 100 km north of the front; 3) Kaoshiung (cf. Fig. 2) within 200 km south of the front; 4) presence of low-level jet (LLJ) inside 18°-26°N, 115°-125°E at 850 or 700 hPa; 5) presence of mesolow near Taiwan; 6) Taiwan inside a low pressure zone; and 7) the mean sea-level pressure in Taiwan is below 1005 hPa. The results (Fig. 12) indicate that among the seven items, an average of 4.15 items are met in group A+, and this figure gradually declines toward smaller groups, from 3.67 in A, 2.84 in B, and finally to only 0.87 in X. Thus, as expected, the synoptic and meso-α-scale conditions tend to be more favorable in larger events. Such conditions, in combination with orographic forcing in Taiwan, appear to favor good model performance, given a sufficient resolution.

https://doi.org/10.5194/nhess-2020-397
Preprint. Discussion started: 22 February 2021

Natural Hazards and Earth System Sciences
Discussions

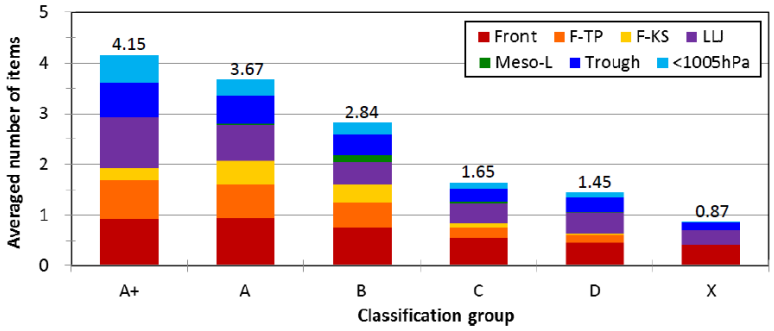

545 **Figure 12.** The average number in the seven items on the checklist met at the starting time of 24-h segments in
546 different classification groups, from A+, A to D, and X, with the proportion of each item plotted and the total
547 number labeled on top. Following the order (bottom to top), the seven items are: presence of surface mei-yu front
548 (front), front near Taipei (F-TP), front near Kaoshiung (F-KS), presence of LLJ, mesolow (meso-L), Taiwan inside a
549 low pressure zone (trough), and the mean sea-level pressure lower than 1005 hPa (<1005 hPa), respectively.
550

551 ## 6 Summary and Concluding Remarks

552 In this section, our results are briefly summarized and the concluding remarks are given. In
553 the mei-yu seasons of 2012-2014, the overall TSs of day-1 QPFs for all events (no classification)
554 by the 2.5-km CReSS are 0.18, 0.15 and 0.09, respectively, at thresholds of 100, 250, and 500
555 mm. The corresponding TSs on day 2 are 0.13, 0.10 and 0.06, and 0.10, 0.03 and 0.00 on day 3.
556 Compared to previous results for mei-yu season in Taiwan (e.g., Hsu et al., 2014; Li and Hong,
557 2014; Su et al., 2016; Huang et al., 2016) and those from contemporary 5-km models, the results
558 herein show significant improvements by the 2.5-km CReSS, especially over the heavy-rainfall
559 thresholds at 130 mm and above. Moreover, when proper classification based on observed rain-
560 area size (i.e., event magnitude) are used, the CRM's ability to predict the extreme and top
561 events (group A+) are much higher, often by a factor of 2 or above in TS. For the top 4% and
562 most hazardous mei-yu events, our day-1 QPFs have TSs of 0.34, 0.24, and 0.16 at the same
563 thresholds of 100, 250, and 500 mm, respectively. The corresponding TSs are 0.32, 0.15 and
564 0.07 on day 2, and 0.25, 0.05 and 0.00 on day 3. Also, the QPFs for larger groups have higher
565 POD, lower FAR, and higher TS than smaller ones, across nearly all thresholds at all ranges of
566 days 1-3. Thus, the positive dependency in categorical scores on the overall rainfall amount also
567 exists in mei-yu regime in Taiwan, as predicted by W15 (and W16).

https://doi.org/10.5194/nhess-2020-397
Preprint. Discussion started: 22 February 2021


Natural Hazards and Earth System Sciences Discussions

568 The improved performance by the 2.5-km CReSS in Taiwan, as shown by an example case,
569 lies in an improved ability to capture the phase-locked topographic rainfall at its correct location
570 in big events toward the extreme thresholds (350-500 mm). For mountain rainfall, it is more
571 predictable using a CRM that also better resolves the terrain (e.g., also Walser and Schär, 2004;
572 Roberts and Lean, 2007), and such QPFs with high hit rates are clearly very useful for hazard
573 mitigation. In contrast, the concentrated rainfall caused by transient systems (such as frontal
574 squall lines) has low predictability due to nonlinearity, and is notoriously difficult and highly
575 random to forecast at the correct location even though a realistic scenario is produced and the
576 potential of heavy rainfall indicated, unless at short-enough ranges. For such rainfall, model
577 QPFs are still informative and useful, but the categorical statistics may not be. As the high-
578 resolution models may possess a higher QPF skill in categorical statics for extreme events than
579 ordinary ones, at least for regions like Taiwan as demonstrated here (and in W15), it is also
580 recommended that such events should be examined with caution and proper classification.
581

582 **Code and data availability**

583 The model used in this study is called Cloud-Resloving Storm Simulator and its website for
584 downloading model and user's guide is at http://www.rain.hyarc.nagoya-
585 u.ac.jp/~tsuboki/cress_html/index_cress_eng.html. And the rainfall figures of Model is at the
586 website http://cressfcst.es.ntnu.edu.tw/.
587

588 **Author contribution**

589 Chung-Chieh Wang designed the experiments and Pi-Yu Chuang carried them out. Chih-
590 Sheng Chang operated the real-time model forecasting and Kazuhisa Tsuboki created the model
591 code. Shin-Yi Huang helped with some figures and Guo-Chen Leu provided some CWB results.
592 Chung-Chieh Wang prepared the manuscript with contributions from all co-authors.
593

594 **Competing interests**

595 The authors declare that they have no conflict of interest.
596

https://doi.org/10.5194/nhess-2020-397
Preprint. Discussion started: 22 February 2021


Natural Hazards and Earth System Sciences Discussions

Acknowledgments

The first author, CCW, wishes to thanks assistants Ms. Y.-W. Wang, Mr. T.-C. Lin, and Mr. K.-Y. Chen for their help on this study. The CWB is acknowledged for providing the observational data, the radar plots, and the QPF verification results in Fig. 5. The National Center for High-performance Computing (NCHC) and the Taiwan Typhoon and Flood Research Institute (TTFRI) provided the computational resources. This study is jointly supported by the Ministry of Science and Technology of Taiwan under Grants MOST-103-2625-M-003-001-MY2, MOST-105-2111-M-003-003-MY3, MOST-108-2111-M- 003-005-MY2, and MOST-109-2625-M-003-001.

References

Barnes, L. R., Schultz, D. M., Gruntfest, E. C., Hayden, M. H., and Benight, C. C.: Corrigendum: False alarm rate or false alarm ratio?, Weather Forecast., 24, 1452–1454, https://doi.org/10.1175/2009WAF2222300.1, 2009.

Bryan, G. H., Wyngaard, J. C., and Fritsch, J. M.: Resolution requirements for the simulation of deep moist convection, Mon. Weather Rev., 131, 2394–2416, https://doi.org/10.1175/1520-0493(2003)131%3C2394:RRFTSO%3E2.0.CO;2, 2003.

Chang, C.-P., Yeh, T.-C., and Chen, J.-M.: Effects of terrain on the surface structure of typhoons over Taiwan, Mon. Weather Rev., 121, 734–752, https://doi.org/10.1175/1520-0493(1993)121%3C0734:EOTOTS%3E2.0.CO;2, 1993.

Chang, C.-P., Yang, Y.-T., and Kuo, H.-C.: Large increasing trend of tropical cyclone rainfall in Taiwan and the roles of terrain, J. Clim., 26, 4138–4147, https://doi.org/10.1175/JCLI-D-12-00463.1, 2013.

Chen, G. T.-J., Wang, C-C., and Lin, D. T.-W.: Characteristics of low-level jets over northern Taiwan in Mei-yu season and their relationship to heavy rain events, Mon. Weather Rev., 133, 20–43, https://doi.org/10.1175/MWR-2813.1, 2005.

Cheung, K. K. W., Huang, L.-R., and Lee, C.-S.: Characteristics of rainfall during tropical cyclone periods in Taiwan, Nat. Hazards Earth Syst. Sci., 8, 1463–1474, https://doi.org/10.5194/nhess-8-1463-2008, 2008.

https://doi.org/10.5194/nhess-2020-397
Preprint. Discussion started: 22 February 2021

Chi, S.-S.: The Mei-Yu in Taiwan, SFRDEST E-06-MT-03-4, Chung-Shin Engineering Technology Research and Development Foundation, Taipei, Taiwan, 65 pp, 2006. (in Chinese)

Chien, F.-C., and Jou, B. J.-D.: MM5 ensemble mean precipitation in the Taiwan area for three early summer convective (Mei-Yu) seasons, Weather Forecast., 19, 735–750, 2004.

Chien, F.-C., Kuo, Y.-H., and Yang, M.-J.: Precipitation forecast of MM5 in the Taiwan area during the 1998 Mei-yu season, Weather Forecast., 17, 739–754, https://doi.org/10.1175/1520-0434(2002)017%3C0739:PFOMIT%3E2.0.CO;2, 2002.

Chien, F.-C., Liu, Y.-C., and Jou, B. J.-D.: MM5 ensemble mean forecasts in the Taiwan area for the 2003 Mei-yu season, Weather Forecast., 21, 1006–1023, https://doi.org/10.1175/WAF960.1, 2006.

Clark, A. J., Gallus, Jr., W. A., and Chen, T.-C.: Comparison of the diurnal precipitation cycle in convection-resolving and non-convection-resolving mesoscale models, Mon. Weather Rev., 135, 3456–3473, https://doi.org/10.1175/MWR3467.1, 2007.

Clark, A. J., Kain, J. S., Stensrud, D. J., Xue, M., Kong, F., Coniglio, M. C., Thomas, K. W., Wang, Y., Brewster, K., Gao, J., Wang, X., Weiss, S. J., and Du, J.: Probabilistic precipitation forecast skill as a function of ensemble size and spatial scale in a convection-allowing ensemble, Mon. Weather Rev., 139, 1410–1418, https://doi.org/10.1175/2010MWR3624.1, 2011.

Cotton, W. R., Tripoli, G. J., Rauber, R. M., and Mulvihill, E. A.: Numerical simulation of the effects of varying ice crystal nucleation rates and aggregation processes on orographic snowfall, J. Appl. Meteorol. Climatol., 25, 1658–1680, https://doi.org/10.1175/1520-0450(1986)025%3C1658:NSOTEO%3E2.0.CO;2, 1986.

Cuo, L., Pagano, T. C., and Wang, Q. J.: A review of quantitative precipitation forecasts and their use in short- to medium-range streamflow forecasting, J. Hydormeteorol., 12, 713–728, https://doi.org/10.1175/2011JHM1347.1, 2011.

Davis, C., Brown, B., and Bullock, R.: Object-based verification of precipitation forecasts. Part I: Methodology and application to mesoscale rain areas, Mon. Weather Rev., 134, 1772–1784, https://doi.org/10.1175/MWR3145.1, 2006.

Deardorff, J. W.,: Stratocumulus-capped mixed layers derived from a three-dimensional model, Bound.-Layer Meteorol., 18, 495–527, 1980.

https://doi.org/10.5194/nhess-2020-397
Preprint. Discussion started: 22 February 2021


Natural Hazards and Earth System Sciences Discussions

656 Done, J., Davis, C. A., and Weisman, M.: The next generation of NWP: explicit forecasts of
657 convection using the weather research and forecasting (WRF) model, *Atmos. Sci. Lett.*, *5*,
658 110–117, 2004.
659 Ebert, E. E.: Ability of a poor man's ensemble to predict the probability and distribution of
660 precipitation, Mon. Weather Rev., 129, 2461–2480, https://doi.org/10.1175/1520-
661 0493(2001)129%3C2461:AOAPMS%3E2.0.CO;2, 2001.
662 Ebert, E. E., and McBride, J. L.: Verification of precipitation in weather systems: Determination
663 of systematic errors, J. Hydrol., 239, 179–202, https://doi.org/10.1016/S0022-
664 1694(00)00343-7, 2000.
665 Ebert, E. E., Damrath, U., Wergen, W., and Baldwin, M. E.: The WGNE assessment of short-
666 term quantitative precipitation forecasts (QPFs) from operational numerical weather
667 prediction models, Bull. Am. Meteorol. Soc., 84, 481–492, https://doi.org/10.1175/BAMS-
668 84-4-481, 2003.
669 Fang, X., and Kuo, Y.-H.: Improving ensemble-based quantitative precipitation forecasts for
670 topography-enhanced typhoon heavy rainfall over Taiwan with a modified probability-
671 matching technique, Mon. Weather Rev., 141, 3908–3932, https://doi.org/10.1175/MWR-
672 D-13-00012.1, 2013.
673 Fritsch, J. M., and Carbone, R. E.: Improving quantitative precipitation forecasts in the warm
674 season. A USWRP research and development strategy, Bull. Am. Meteorol. Soc., 85, 955–
675 965, https://doi.org/10.1175/BAMS-85-7-955, 2004.
676 Gilleland, E., Ahijevych, D. A., Brown, B. G., and Ebert, E. E.: Verifying forecasts spatially,
677 Bull. Am. Meteorol. Soc., 91, 1365–1373, https://doi.org/10.1175/2010BAMS2819.1, 2010.
678 Golding, B. W.: Quantitative precipitation forecasting in the UK. J. Hydrol., 239, 286–305,
679 https://doi.org/10.1016/S0022-1694(00)00354-1, 2000.
680 Hong, J.-S.: Evaluation of the high-resolution model forecasts over the Taiwan area during
681 GIMEX, Weather and Forecast., 18, 836–846, https://doi.org/10.1175/1520-
682 0434(2003)018%3C0836:EOTHMF%3E2.0.CO;2, 2003.
683 Hong, J.-S., Fong, C.-T., Hsiao, L.-F., Yu, Y.-C., and Tseng, C.-Y.: Ensemble typhoon
684 quantitative precipitation forecasts model in Taiwan, Weather Forecast., 30, 217–237,
685 https://doi.org/10.1175/WAF-D-14-00037.1, 2015.
686 Hsu, J.: ARMTS up and running in Taiwan, Väisälä News, 146, 24–26, 1998.

https://doi.org/10.5194/nhess-2020-397
Preprint. Discussion started: 22 February 2021


Natural Hazards and Earth System Sciences Discussions

687 Hsu, J. C.-S., Wang, C.-J., Chen, P.-Y., Chang, T.-H., and Fong, C.-T. (2014), Verification of
688 quantitative precipitation forecasts by the CWB WRF and ECMWF on 0.125° grid, in:
689 Proceedings of 2014 Conference on Weather Analysis and Forecasting, Central Weather
690 Bureau, Taipei, Taiwan, 16-18 September 2014, A2-24, 2014. (in Chinese)
691 Huang, T.-S., Yeh, S.-H., Leu, G.-C., and Hong, J.-S.:, A synthesis and comparison of QPF
692 verifications at the CWB and major NWP guidance, in: Proceedings of 2015 Conference on
693 Weather Analysis and Forecasting, Central Weather Bureau, Taipei, Taiwan, 15-17
694 September 2015, A7-11, 2015. (in Chinese)
695 Huang, T.-S., Yeh, S.-H., Leu, G.-C., and Hong, J.-S.: Postprocessing of ensemble rainfall
696 forecasts---Ensemble mean, probability matched mean and exceeding probability,
697 Atmospheric Sciences, 44, 173–196, 2016. (in Chinese with English abstract)
698 Ikawa, M., and Saito, K: Description of a non-hydrostatic model developed at the Forecast
699 Research Department of the MRI, Technical Report, 28, Meteorological Research Institute,
700 Tsukuba, Ibaraki, Japan, 245 pp, 1991.
701 Jou, B. J.-D., Lee, W.-C., and Johnson, R. H.: An overview of SoWMEX/TiMREX, in: The
702 Global Monsoon System: Research and Forecast, 2nd Edition, edited by: Chang, C.-P.,
703 Ding, Y., Lau, N.-C., Johnson, R. H., Wang, B., Yasunari, T., World Scientific, Toh Tuck
704 Link, Singapore, 303–318, https://doi.org/10.1142/9789814343411_0018, 2011.
705 Kalnay, E., Kanamitsu, M., and Baker, W. E.: Global numerical weather prediction at the
706 National Meteorological Center, Bull. Am. Meteorol. Soc., 71, 1410–1428, 1990.
707 Kanamitsu, M.: Description of the NMC global data assimilation and forecast system, Weather
708 Forecast., 4, 335–342, https://doi.org/10.1175/1520-
709 0434(1989)004%3C0335:DOTNGD%3E2.0.CO;2, 1989.
710 Kleist, D. T., Parrish, D. F., Derber, J. C., Treadon, R., Wu, W. S., and Lord, S.: Introduction of
711 the GSI into the NCEP global data assimilation system, Weather Forecast., 24, 1691–1705,
712 https://doi.org/10.1175/2009WAF2222201.1, 2009.
713 Kondo, J.: Heat balance of the China Sea during the air mass transformation experiment, J.
714 Meteor. Soc. Japan, 54, 382–398, https://doi.org/10.2151/jmsj1965.54.6_382, 1976.
715 Kuo, Y.-H., and Chen, G. T.-J.: The Taiwan Area Mesoscale Experiment (TAMEX): An
716 overview, Bull. Am. Meteorol. Soc., 71, 488–503, http://dx.doi.org/10.1175/1520-
717 0477(1990)071%3C0488:TTAMEA%3E2.0.CO;2, 1990.

https://doi.org/10.5194/nhess-2020-397
Preprint. Discussion started: 22 February 2021

718 Li, C.-H., and Hong, J.-S.: Study on the application and analysis of regional ensemble
719 quantitative precipitation forecasts, in: Proceedings of 2014 Conference on Weather
720 Analysis and Forecasting, Central Weather Bureau, Taipei, Taiwan, 16-18 September 2014,
721 A2-19, 2014. (in Chinese)
722 Li, J. and Chen, Y.-L.: Barrier jets during TAMEX, Mon. Weather Rev., 126, 959–971,
723 https://doi.org/10.1175/1520-0493(1998)126%3C0959:BJDT%3E2.0.CO;2, 1998.
724 Lin, Y.-L., Farley, R. D., and Orville, H. D.: Bulk parameterization of the snow field in a cloud
725 model, J. Appl. Meteorol. Climatol., 22, 1065–1092, https://doi.org/10.1175/1520-
726 0450(1983)022%3C1065:BPOTSF%3E2.0.CO;2, 1983.
727 Louis, J. F., Tiedtke, M., and Geleyn, J. F.: A short history of the operational PBL
728 parameterization at ECMWF, in: Proceedings of Workshop on Planetary Boundary Layer
729 Parameterization, Shinfield Park, Reading, UK, 25-27 November 1981, 59–79, 1982.
730 Moorthi, S., Pan, H. L., and Caplan, P.: Changes to the 2001 NCEP operational MRF/AVN
731 global analysis/forecast system, NWS Technical Procedures Bulletin, 484, Office of
732 Meteorology, National Weather Service, Silver Spring, Maryland, USA, 2001.
733 Murakami, M.: Numerical modeling of dynamical and microphysical evolution of an isolated
734 convective cloud---The 19 July 1981 CCOPE cloud, J. Meteor. Soc. Japan, 68, 107–128,
735 https://doi.org/10.2151/jmsj1965.68.2_107, 1990.
736 Murakami, M., Clark, T. L., and Hall, W. D.: Numerical simulations of convective snow clouds
737 over the Sea of Japan: Two-dimensional simulation of mixed layer development and
738 convective snow cloud formation, J. Meteor. Soc. Japan, 72, 43–62,
739 https://doi.org/10.2151/jmsj1965.72.1_43, 1994.
740 Roberts, N. M., and Lean, H. W.: Scale-selective verification of rainfall accumulations from
741 high-resolution forecasts of convective events, Mon. Weather Rev., 136, 78–97,
742 https://doi.org/10.1175/2007MWR2123.1, 2007.
743 Roebber, P. J.: Visualizing multiple measures of forecast quality, Weather Forecast., 24, 601–
744 608, https://doi.org/10.1175/2008WAF2222159.1, 2009.
745 Schaefer, J. T.: The critical success index as an indicator of warning skill, Weather Forecast., 5,
746 570–575, https://doi.org/10.1175/1520-0434(1990)005%3C0570:TCSIAA%3E2.0.CO;2,
747 1990.

https://doi.org/10.5194/nhess-2020-397
Preprint. Discussion started: 22 February 2021


Natural Hazards and Earth System Sciences Discussions

748 Segami, A., Kurihara, K., Nakamura, H., Ueno, M., Takano, I., and Tatsumi, Y.: Operational
749 mesoscale weather prediction with Japan Spectral Model, J. Meteor. Soc. Japan, 67, 907–
750 924, https://doi.org/10.2151/jmsj1965.67.5_907, 1989.
751 Skamarock, W. C., Klemp, J. B., Dudhia, J., Gill, D. O., Barker, D. M., Wang, W., and Powers,
752 J. G.: A description of the advanced research WRF version 2, National Center for
753 Atmospheric Reasearch, Boulder, Colorado, USA, 88 pp,
754 http://dx.doi.org/10.5065/D6DZ069T, 2005.
755 Su, Y.-J., Hong, J.-S., and Li, C.-H.: The characteristics of the probability matched mean QPF
756 for 2014 Meiyu season, Atmospheric Sciences, 44, 113-134, 2016. (in Chinese with English
757 abstract)
758 Tsuboki, K., and Sakakibara, A.: Large-scale parallel computing of cloud resolving storm
759 simulator, in: High Performance Computing, edited by: Zima H. P., Joe K., Sato M., Seo
760 Y., Shimasaki M., Springer, Berlin, Heidelberg, Germany, 243–259,
761 https://doi.org/10.1007/3-540-47847-7_21, 2002.
762 Tsuboki, K., and Sakakibara, A.: Numerical Prediction of High-Impact Weather Systems: The
763 Textbook for the Seventeenth IHP Training Course in 2007, Hydrospheric Atmospheric
764 Research Center, Nagoya University, Nagoya, Japan, and UNESCO, Paris, France, 273 pp,
765 2007.
766 Walser, A., and Schär, C.: Convection-resolving precipitation forecasting and its predictability in
767 Alpine river catchments, J. Hydrol., 288, 57–73,
768 https://doi.org/10.1016/j.jhydrol.2003.11.035, 2004.
769 Wang, C.-C.: On the calculation and correction of equitable threat score for model quantitative
770 precipitation forecasts for small verification areas: The example of Taiwan, Weather
771 Forecast., 29, 788–798, https://doi.org/10.1175/WAF-D-13-00087.1, 2014.
772 Wang, C.-C.: The more rain, the better the model performs—The dependency of quantitative
773 precipitation forecast skill on rainfall amount for typhoons in Taiwan, Mon. Weather Rev.,
774 143, 1723–1748, https://doi.org/10.1175/MWR-D-14-00137.1, 2015.
775 Wang, C.-C.: News and notes, Paper of notes: The more rain from typhoons, the better the
776 models perform, Bull. Am. Meteorol. Soc., 97, 16–17,
777 https://doi.org/10.1175/BAMS_971_11-18_Nowcast, 2016.

https://doi.org/10.5194/nhess-2020-397
Preprint. Discussion started: 22 February 2021


Natural Hazards and Earth System Sciences Discussions

778 Wang, C.-C., Chen, G. T.-J., Chen, T.-C., and Tsuboki, K.: A numerical study on the effects of
779 Taiwan topography on a convective line during the mei-yu season, Mon. Weather Rev.,
780 133, 3217–3242, https://doi.org/10.1175/MWR3028.1, 2005.
781 Wang, C.-C., Chen, G. T.-J., and Huang, S.-Y.: Remote trigger of deep convection by cold
782 outflow over the Taiwan Strait in the Mei-yu season: A modeling study of the 8 June 2007
783 Case, Mon. Weather Rev., 139, 2854–2875, https://doi.org/10.1175/2011MWR3613.1,
784 2011.
785 Wang, C.-C., Kung, C.-Y., Lee, C.-S., and Chen, G. T.-J.: Development and evaluation of Mei-
786 yu season quantitative precipitation forecast in Taiwan river basins based on a conceptual
787 climatology model, Weather Forecast., 27, 586–607, https://doi.org/10.1175/WAF-D-11-
788 00098.1, 2012a.
789 Wang, C.-C., Kuo, H.-C., Chen, Y.-H., Huang, H.-L., Chung, C.-H., and Tsuboki, K.: Effects of
790 asymmetric latent heating on typhoon movement crossing Taiwan: The case of Morakot
791 (2009) with extreme rainfall, J. Atmos. Sci., 69, 3172–3196, https://doi.org/10.1175/JAS-D-
792 11-0346.1, 2012b.
793 Wang, C.-C., Chen, Y.-H., Kuo, H.-C., and Huang, S.-Y.: Sensitivity of typhoon track to
794 asymmetric latent heating/rainfall induced by Taiwan topography: A numerical study of
795 Typhoon Fanapi (2010), J. Geophys. Res. Atmos., 118, 3292–3308,
796 https://doi.org/10.1002/jgrd.50351, 2013a.
797 Wang, C.-C., Kuo, H.-C., Yeh, T.-C., Chung, C.-H., Chen, Y.-H., Huang, S.-Y., Wang, Y.-W.,
798 and Liu, C.-H.: High-resolution quantitative precipitation forecasts and simulations by the
799 Cloud-Resolving Storm Simulator (CReSS) for Typhoon Morakot (2009), J. Hydrol., 506,
800 26–41. https://doi.org/10.1016/j.jhydrol.2013.02.018, 2013b.
801 Wang, C.-C., Huang, S.-Y., Chen, S.-H., Chang, C.-S., and Tsuboki, K.: Cloud-resolving
802 typhoon rainfall ensemble forecasts for Taiwan with large domain and extended range
803 through time-lagged approach, Weather Forecast., 31, 151–172,
804 https://doi.org/10.1175/WAF-D-15-0045.1, 2016a.
805 Wang, C.-C., Chiou, B.-K., Chen, G. T.-J., Kuo, H.-C., and Liu, C.-H.: A numerical study of
806 back-building process in a quasistationary rainband with extreme rainfall over northern
807 Taiwan during 11-12 June 2012, Atmos. Chem. Phys., 16, 12359–12382,
808 https://doi.org/10.5194/acp-16-12359-2016, 2016b.

https://doi.org/10.5194/nhess-2020-397
Preprint. Discussion started: 22 February 2021

809 Wang, C.-C., Paul, S., Chien, F.-C., Lee, D.-I., and Chuang, P.-Y.: An evaluation of WRF
810 rainfall forecasts in Taiwan during three mei-yu seasons of 2008-2010, Weather Forecast.,
811 32, 1329–1351, https://doi.org/10.1175/WAF-D-16-0190.1, 2017.
812 Wernli, H., Paulat, M., Hagen, M., and Frei, C.: SAL—A novel quality measure for the
813 verification of quantitative precipitation forecasts, Mon. Weather Rev., 136, 4470–4487,
814 https://doi.org/10.1175/2008MWR2415.1, 2008.
815 Wilks, D. S.: Statistical methods in the atmospheric sciences, 3rd Edition. Academic Press, San
816 Diego, California, USA, 2011.
817 Wu, C.-C., and Kuo, Y.-H.: Typhoons affecting Taiwan: Current understanding and future
818 challenges, Bull. Am. Meteorol. Soc., 80, 67–80, https://doi.org/10.1175/1520-
819 0477(1999)080%3C0067:TATCUA%3E2.0.CO;2, 1999.
820 Yang, M.-J., Jou, B. J.-D., Wang, S.-C., Hong, J.-S., Lin, P.-L., Teng, J.-H., and Lin, H.-C.:
821 Ensemble prediction of rainfall during the 2000–2002 mei-yu seasons: Evaluation over the
822 Taiwan area, J. Geophys. Res., 109, D18203, https://doi.org/10.1029/2003JD004368, 2004.
823 Yeh, H.-C., and Chen, Y.-L.: Characteristics of the rainfall distribution over Taiwan during
824 TAMEX, J. Appl. Meteorol. Climatol., 37, 1457–1469, https://doi.org/10.1175/1520-
825 0450(1998)037%3C1457:CORDOT%3E2.0.CO;2, 1998.
826 Yeh, H.-C., and Chen, Y.-L.: The role of off shore convergence on coastal rainfall during
827 TAMEX IOP 3, Mon. Weather Rev., 130, 2709–2730, https://doi.org/10.1175/1520-
828 0493(2002)130%3C2709:TROOCO%3E2.0.CO;2, 2002.